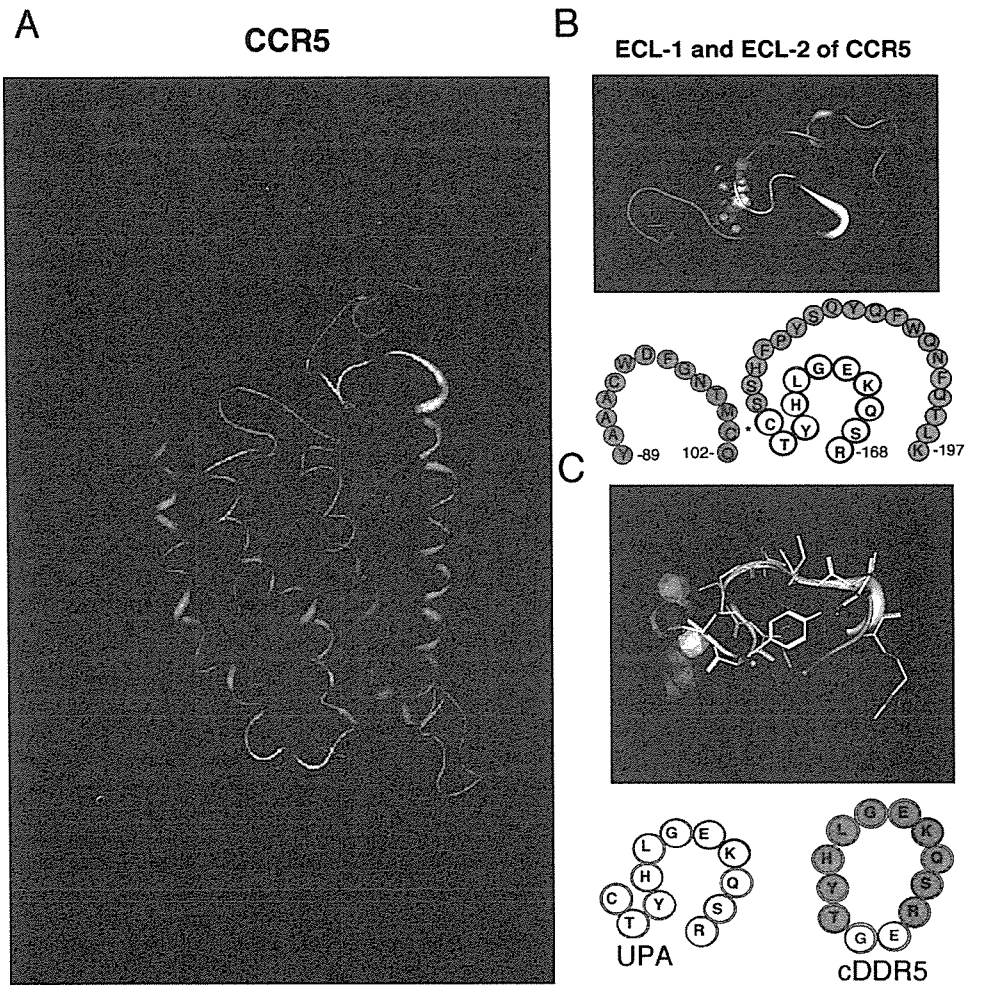

FIGURE 1. Deduced structure of UPA in extracellular loop-2 of CCR5. *A*, The predicted model of CCR5 was constructed using the segmented approach, and MOE was used for actual calculation. The determined structure of rhodopsin was used as the template. Transmembrane helixes are in cyan. The extracellular loops of CCR5 are color coded: N terminus, blue; extracellular loop-1, green; extracellular loop-2, yellow-orange; UPA, yellow; and extracellular loop-3, magenta. The intercellular loops are in gray, and the C terminus is in red. *B*, Predicted model of UPA in CCR5. Because cysteine residues in extracellular loop-1 and extracellular loop-2 form a disulfide bond, the extracellular loop-2 region of CCR5 has a unique arch structure consisting of 11 aa residues (yellow). In this study, UPA was selected as the target of peptide immunogen. *C*, To mimic the deduced conformational epitope of UPA in CCR5, the decapeptide (R_{168}SQKEGLHYT_{177}) derived from the UPA sequence was cyclized by inserting the spacer-armed dipeptide (Gly-Glu), and the deduced structure of cDDR5 (in cyan) was adopted as the deduced structural model of UPA in CCR5 using the MOE-Align tool.

separately conjugated to the MAP resin (Applied Biosystems) and 5-[5-(*N*-succinimidyloxycarbonyl)pentylamido]hexyl D-biotinamide through ethylenediamine. cDDR5 derivatives, in which all protected groups were removed using trifluoroacetic acid, were used for the following purposes. cDDR5-MAP was used to immunize cynomolgus macaques. MAP is commercially available (Applied Biosystems) and is composed of a 2-fold bifurcating polylysine core developed as a carrier of a peptide Ag. In contrast, biotinylated cDDR5 was used to confirm the specific binding of Abs to cDDR5 using a BIAcore biosensor. Unless otherwise specified, all of the peptides used were purified by HPLC (Waters), and the molecular masses of the compounds were determined by MALDI-TOF mass spectrometry (Burker Franzen Analytik).

Immunization schedule

All of the cynomolgus macaques were housed in individual cages and maintained according to the rules and guidelines of the National Institute for Infectious Diseases for experimental animal welfare. In the pilot test, a 4-year-old cynomolgus macaque was immunized i.p. at 0 and 1 wk with 300 μg of cDDR5-MAP in CFA and boosted s.c. at 6 wk with 300 μg of cDDR5-MAP in IFA. Furthermore, three 4- to 6-year-old cynomolgus macaques (nos. 11, 13, and 16) were also immunized with cDDR5-MAP according to the same schedule. Another three cynomolgus macaques (nos. 7–9) were immunized with MAP following the same immunization schedule as the controls. Immune sera were obtained at 0, 1, 2, 4, 6, 8, 10, and 21 wk postinitial immunization (wpim), and were then subjected to BIAcore analysis and MAGIC-5 assay.

Real-time biomolecular interaction analysis using surface plasmon resonance

The principle in analyzing Ag-Ab interactions has been described (10). Biotinylated cDDR5 was injected into a streptavidin-coated sensor chip (BIAcore KK). Binding experiments were performed by injecting immune sera diluted 1/9 with PBS (0.02% KH_2PO_4, 0.29% $Na_2HPO_4{}'12H_20$, 0.8% NaCl, and 0.02% KCl).

Flow cytometry

CEM-CCR5 cells (22) were washed with PBS and then suspended in a cold washing buffer (PBS containing 2% FBS and 0.02% NaN_3) at 1×10^6

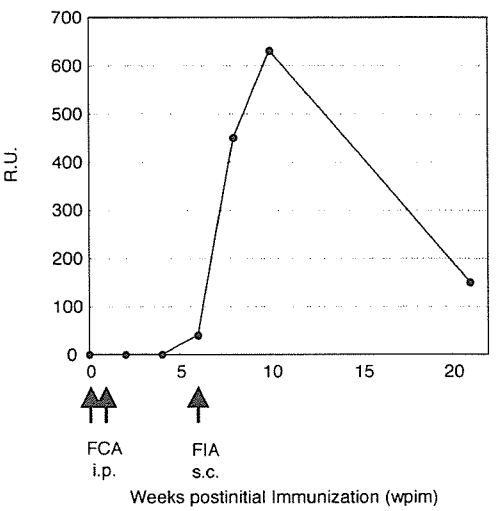

FIGURE 2. Induction of cDDR5-specific Abs after immunization with cDDR5-MAP in cynomolgus macaques. Serum samples obtained before and after immunization with cDDR5-MAP (at 0, 1, 2, 4, 6, 8, 10, and 21 wpim) were examined to investigate whether the antisera against the moiety of cDDR5 can be raised in cynomolgus macaques using real-time biomolecular interaction analysis using surface plasmon resonance with a biotinylated cDDR5-bound BIAcore biosensor.

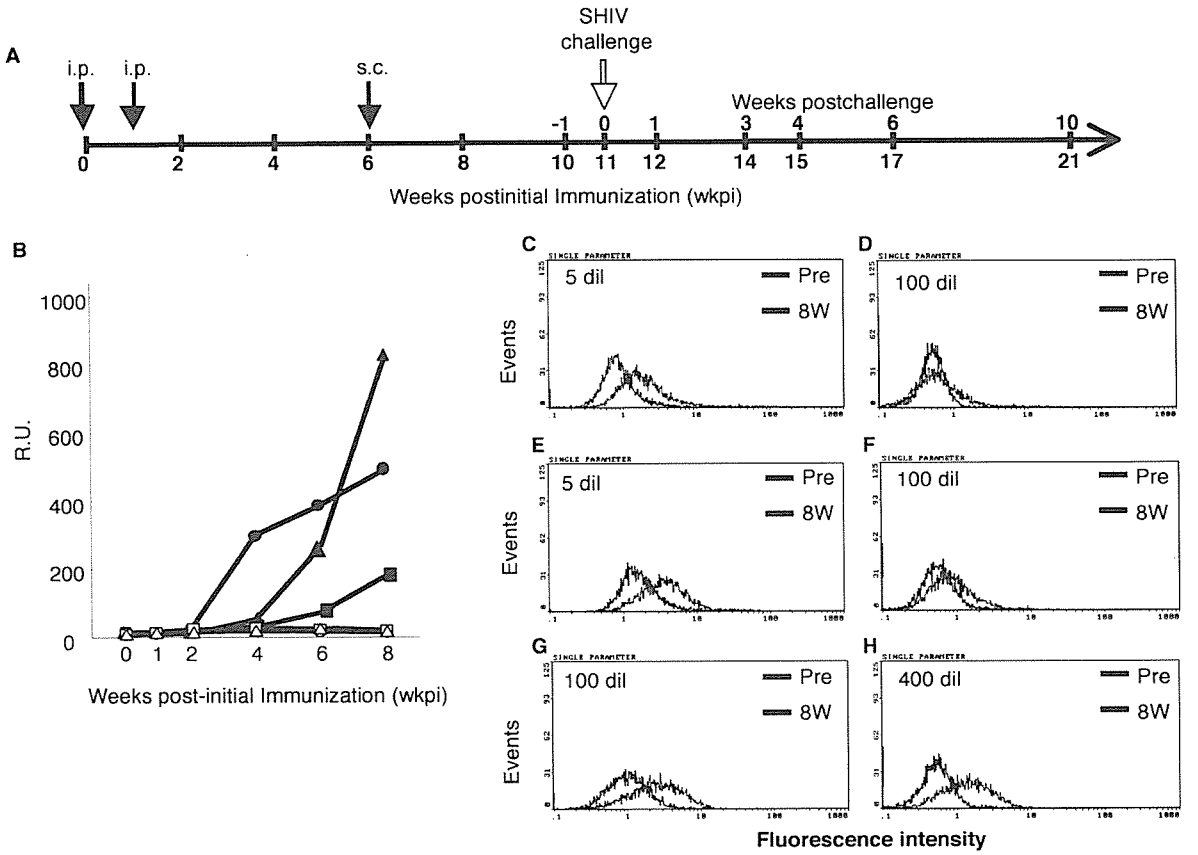

FIGURE 3. Immunization schedule and detection of anti-CCR5 Abs in cynomolgus macaques. *A*, Immunization schedule for cynomolgus macaques. Three cynomolgus macaques (nos. 11, 13, and 16) were immunized i.p. at 0 and 1 wk with 300 μg of cDDX4-MAP, and boosted s.c. at 6 wk with 300 μg of cDDR5-MAP. Another three cynomolgus macaques (nos. 7, 8, and 9) were immunized with MAP as the control. Blood sampling was performed at 0, 1, 2, 4, 6, 8, 10, 12, 14, 15, 17, and 21 wpim. *B*, Detection of anti-cDDR5-MAP serum Abs in cynomolgus macaques. Serum samples obtained before and after immunization with cDDR5-MAP (macaque nos. 11 (○), 13 (■), and 16 (▲) or MAP (macaque nos. 7 (○), 8 (□), and 9 (△) were examined to investigate whether the antisera against the moiety of cDDR5 can be raised in cynomolgus macaques. The anti-cDDR5 macaque Abs from each serum sample were detected by real-time biomolecular interaction analysis using surface plasmon resonance with a biotinylated cDDR5-bound BIAcore biosensor, as shown in Fig. 2. Sensorgrams from the serum samples taken before and after immunization were obtained, and the highest response units (R.Us.) in each sample were plotted. *C–H*, Flow cytometry of serum Abs from cynomolgus macaques (no. 11, *C* and *D*; no. 13, *E* and *F*; no. 16, *G* and *H*) immunized with cDDR5-MAP. CEM-CCR5 cells were subjected to flow cytometry, as described in *Materials and Methods*, in which the cells were separately incubated with the preimmunization (dark blue histogram) and 8 wpim (red histogram) sera diluted 1/5, 1/100, or 1/400 with PBS. The dilution folds are shown as 5, 100, or 400 dil in each figure. Significant binding to a cell was determined positive when the mean fluorescence intensity ratio of 8 wpim serum to 0 wpim serum is >1.5.

cells/ml. The cells were incubated with preimmunization and 8 wpim sera, which were dialyzed using Spectra/Por (cutoff molecular mass, 100,000; Spectrum Laboratories), according to the manufacturer's instructions, and diluted 1/5, 1/100, or 1/400 with PBS. Because immunization with the extracellular linear peptide of CCR5 up-regulates the concentrations of CCL5, CCL3, and CCL4, which are CCR5 ligands (11), the sera were dialyzed and then diluted with PBS for flow cytometry. The cells were resuspended in the washing buffer containing FITC-conjugated anti-monkey Ig (IgG, IgA, and IgM) Abs (H&L) (Rockland). After 30 min of incubation at 4°C, the cells were washed three times and then analyzed using an EPICS XL flow cytometer (Beckman Coulter).

The specificity of anti-cDDR5 serum for native CCR5 expressed on cynomolgus macaque PBMCs or HSC-F (23) was tested by examining the ability of anti-cDDR5 serum to block binding of a CCR5-specific mAb (3A9; BD Pharmingen). A total of 1×10^6 cells was incubated with pre-immunization or 10 wpim serum, which was dialyzed and diluted (1/2) with PBS, from vaccinated macaques no. 16 for 15 min at room temperature. The cells were washed and then stained with FITC-labeled anti-CD95 (BD Pharmingen) and PE-labeled anti-CCR5 (3A9; BD Pharmingen) for 20 min at room temperature. Finally, the cells were washed again and then analyzed using an EPICS XL flow cytometer. Control experiments were conducted without preincubation with preimmunization or 10 wpim serum.

MAGIC-5 assay

The antiviral activity of the sera obtained before and after immunization with cDDR5-MAP was determined using MAGIC-5 cells, as previously described (10). MAGIC-5 cells were plated at 1×10^4 cells/well (96-well plates) and incubated overnight in RPMI 1640 containing 5% FCS (200 μl); the medium was then replaced with the preimmunization and 8 wpim sera (30 μl), which were dialyzed using Spectra/Por, and serially diluted (1/5–1/1280) with PBS. The cells were then separately incubated in suspensions of R5 and X4 clade B viruses, nonclade B primary isolates, or simian/HIV (SHIV) (10 μl: HIV_{LAV-1}, 5077; HIV_{JRFL}, 3749; $HIV_{93RW004}$, 1406; HIV_{MJ4}, 844; $SHIV_{SF162P3}$, 713 tissue culture infective $dose_{50}$ ($TCID_{50}$)/ml in the presence of 20 μg/ml DEAE dextran for 2 h, and then cocultured in the medium (160 μl) for 48 h. The cells were fixed, and HIV-1-infected cells identified by their blue staining were counted by conventional methods.

Productive infection assay using $SHIV_{SF162P3}$

CEM-CCR5 cells (5×10^5) (22) were infected with $SHIV_{SF162P3}$ (3.2 ng/ml as measured using p27 Ag) in the presence of the preimmunization and 8 wpim sera for 18 h. The cells were washed with PBS, and then plated onto 24-well plates and cultured in 3 ml of the RPMI 1640 medium containing 10% FBS. The culture supernatants 24, 48, 72, 96, and 120 h after

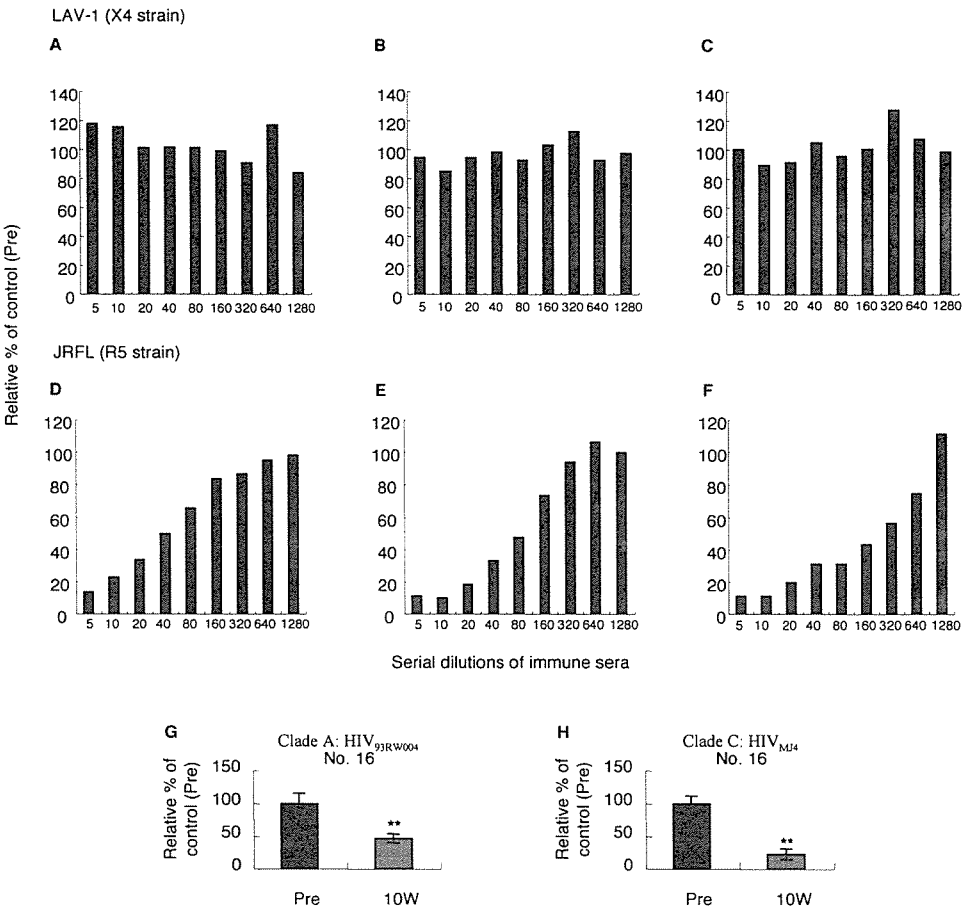

FIGURE 4. Inhibitory effects of pre- and postimmunization sera on HIV-1 R5 and X4 infections. MAGIC-5 cells were separately incubated with serially diluted 8 wpim serum from cDDR5-MAP-immunized macaques (*A* and *D*, no. 11; *B* and *E*, no. 13; *C* and *F*, no. 16). Preimmunization serum was used as control. The cells were further cocultured in a medium containing various HIV-1 strains (*A–C*, LAV-1; *D–F*, JRFL) for 48 h, as described in *Materials and Methods*. The infected cells, which were stained blue, were counted by a conventional method. The number of cells stained blue is expressed as percentage relative to the number of cells in the preimmunization serum (control) stained blue for each macaque. No significant cytotoxicity of the immunization serum-containing medium was observed. Values represent the mean of three determinations. *G* and *H*, MAGIC-5 cells were separately incubated with preimmunization and 10 wpim sera, which were dialyzed and diluted (1/2) with PBS, from vaccinated macaque no. 16. The cells were further cocultured in a medium containing nonclade B HIV-1 strains ($HIV_{93RW004}$, HIV_{MJ4}) for 48 h, as described in *Materials and Methods*.

infection were removed to detect SIV p27 Ag by RETRO-TEK SIV type 1 $p27^{gag}$ Ag ELISA, according to the manufacturer's instructions.

HIV-1 and SHIV strains

Clade B laboratory-adapted strains $HIV\text{-}1_{JRFL}$ and $HIV\text{-}1_{LAV\text{-}1}$ were used. These clade B viruses were propagated in a chronically $HIV\text{-}1_{JRFL}$-infected T cell line (Molt4-CCR5/JRFL) and a chronically $HIV\text{-}1_{LAV\text{-}1}$-infected T cell line (CEM/LAV-1) grown in a complete medium consisting of RPMI 1640 supplemented with 10% heat-inactivated, defined FBS (HyClone), penicillin (100 IU/ml), and streptomycin (0.1 mg/ml). The nonclade B strains $HIV_{93RW004}$ and HIV_{MJ4} (AIDS Research and Reference Reagent Program, Division of AIDS, National Institute of Allergy and Infectious Diseases, National Institutes of Health) were propagated in 3-day-cultured, PHA-activated human PBMCs. Furthermore, $SHIV\text{-}1_{SF162P3}$ (24, 25) (AIDS Research and Reference Reagent Program, Division of AIDS, National Institute of Allergy and Infectious Diseases, National Institutes of Health) was similarly propagated in 3-day-cultured, PHA-activated cynomolgus macaque PBMCs. Each cell-free virus stock was prepared from tissue culture supernatants harvested from chronically and acutely infected cells. Virus-containing supernatants were pooled, filtered through a 0.45-μm membrane, aliquoted, and frozen to provide a uniform stock of infectious virus.

Macaque challenge

All of the six cynomolgus macaques were i.v. challenged with 1 ml of 10 $TCID_{50}$/ml $SHIV_{SF162P3}$. Blood, serum, and plasma samples were collected from the infected animals at regular intervals after infection.

Determination of SHIV RNA viral load by SYBR green-based quantitative real-time PCR assay

Viral RNA was extracted from plasma using a QIAamp viral RNA minikit (Qiagen), then retrotranscribed using the SuperScript III First-Strand Synthesis system (Invitrogen Life Technologies). cDNA duplicates were amplified by SYBR green real-time PCR assay previously described (26) with some modifications. Briefly, primers that recognize specific and highly conserved sequences on the *gag* region of SIV described by Ui et al. (27) were selected. The sequences of SIV gag primers were 5′-GGAAATTAC CCAGTACAACAAATAGG-3′ and 5′-TCTATCAATTTTACCCAG GCATTTA-3′. The SIV *gag* gene was amplified in 20 μl of a PCR mixture consisting of 10 μl of 2× master mix containing modified DyNAmo hot start DNA polymerase, SYBR green I, optimized PCR buffer, 5 mM $MgCl_2$, a dNTP mix including dUTP (Finnzymes), 2 μl of each primer, and 8 μl of cDNA. PCR was conducted as follows: initial activation of hot start DNA polymerase at 95°C for 15 min; 40 cycles of four steps of 95°C for 10 s, 57°C for 20 s, 72°C for 20 s, and 76°C for 2 s. At the end of the amplification cycle, melting temperature analysis was conducted by gradually increasing the temperature (0.5°C/s) to 95°C. Amplification, data acquisition, and analysis were conducted with the DNA Engine Opticon 2 System (MJ Research) using Opticon Monitor version 2.02 software (MJ Research). The detection limit of this system was 1×10^3 copies/ml.

Results

Design and synthesis of cDDR5

The hypothetical structural model of CCR5 was based on its homology with rhodopsin (28), and was energy minimized using the molecular operating environment (MOE; Chemical Computing Group) (Fig. 1*A*). The extracellular loop-2 region of CCR5 and its structure deduced on the basis of the Cys^{178} residue bound to the Cys^{101} residue of extracellular loop-1 by a disulfide bond using MOE showed a unique arch consisting of 11 aa residues (undecapeptidyl arch (UPA)) (Fig. 1*B*). The cDDR5 moiety designed to mimic the deduced conformational epitope of UPA was generated by the cyclization of a decapeptide (R_{168}SQKEGLHYT_{177}) derived from the UPA sequence by inserting a spacer-armed dipeptide (Gly-Glu). The deduced structure of cDDR5 (shown in cyan) was adopted in the construction of the hypothetical structural

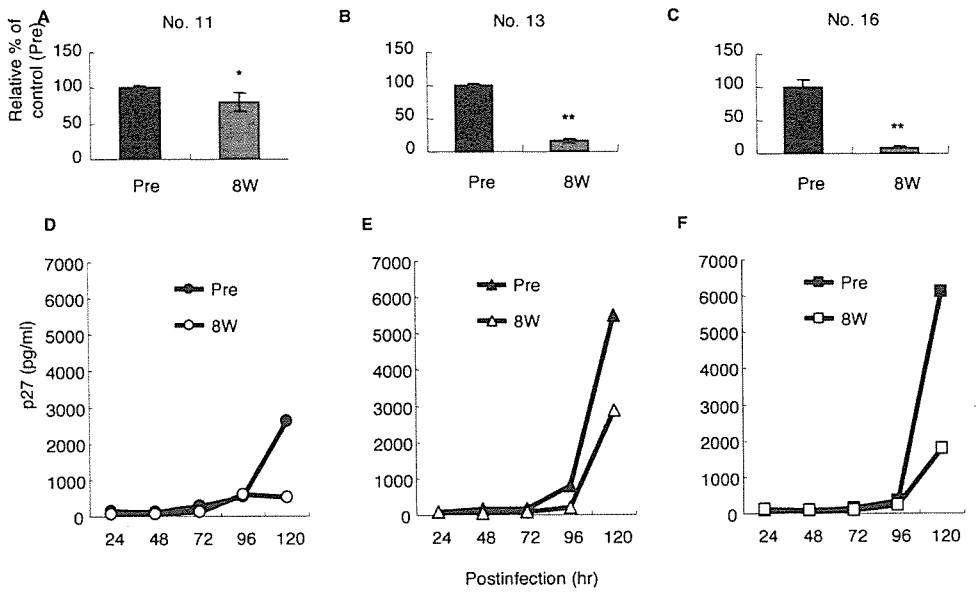

FIGURE 5. Inhibitory effects of pre- and postimmunization sera on CCR5-specific $SHIV_{SF162P3}$ infection. *Upper* and *bottom figures*, Show the results of MAGIC-5 assay (*A*, no. 11; *B*, no. 13; *C*, no. 16) and productive infection assay (*D*, no. 11; *E*, no. 13; *F*, no. 16), respectively. In MAGIC-5 assay, MAGIC-5 cells were separately incubated with preimmunization and 8 wpim sera, which were dialyzed and diluted (1/10) with PBS, and cocultured in the $SHIV_{SF162P3}$-containing medium for 48 h, as described in *Materials and Methods*. The infected cells, which were stained blue, were counted. ■ and ▨, Represent the results from preimmunization and 8 wpim sera, respectively. No significant cytotoxicity of the immunization serum-containing medium was observed. Diluted virus stocks that infected 100–300 cells, as identified by their blue staining, were used. The number of cells stained blue was expressed as percentage relative to the number of cells in the preimmunization sera (control) stained blue. All data represented means obtained from three separate experiments. Statistically significant differences compared with preimmunization serum are indicated by asterisks (*, $p < 0.05$; **, $p < 0.01$). In the productive infection assay, CEM-CCR5 cells (5×10^5) were infected with the $SHIV_{SF162P3}$-containing medium in the presence of preimmunization and 8 wpim sera for 18 h. The cells were washed with PBS, plated onto 24-well plates, and then cultured in the RPMI 1640 medium containing 10% FBS. The p27 Ag in culture supernatants obtained at 24, 48, 72, 96, and 120 h postinfection was detected, as described in *Materials and Methods*. Cynomolgus macaque no. 11, Pre (●) and 8 wk (○); no. 13, Pre (▲) and 8 wk (△); no. 16, Pre (■) and 8 wk (□).

model of UPA in CCR5 (shown in yellow) using the MOE-Align tool (Chemical Computing Group) (Fig. 1*C*).

Induction of cDDR5-specific Abs after immunization with cDDR5-MAP in cynomolgus macaques

We pilot tested whether the immunization of cynomolgus macaques with cDDR5-MAP induces cDDR5-specific Abs. To examine the duration and magnitude of anti-cDDR5 autoantibody induction, a cynomolgus macaque was immunized i.p. at 0 and 1 wk with cDDR5-MAP in CFA and boosted s.c. at 6 wk with cDDR5-MAP in IFA. Ab responses against cDDR5 were measured by real-time biomolecular interaction analysis using surface plasmon resonance. As shown in Fig. 2, the titer of anti-cDDR5 sera measured 4 wk after the third immunization (10 wpim) was the highest in the cynomolgus macaques (titer of ~630 response units). Furthermore, the immunization with cDDR5-MAP induced anti-cDDR5 serum production for ~15 wk after the third immunization, although the titer of anti-cDDR5 sera declined over time until 21 wpim (Fig. 2).

Vaccination of cynomolgus macaques with cDDR5-MAP and induction of CCR5-specific Abs

To verify whether cDDR5-MAP could induce CCR5-specific Abs with anti-HIV-1 activity in nonhuman primates, an experiment was performed using cynomolgus macaques immunized following the time schedule shown in Fig. 3*A*. Three cynomolgus macaques were immunized with cDDR5-MAP in CFA or IFA by i.p. or s.c. injection, as described in Fig. 2. Another three cynomolgus macaques were immunized with MAP as the control. cDDR5-specific Abs were significantly induced in cynomolgus macaque nos. 11, 13, and 16 at 8 wpim (Fig. 3*B*). In contrast, the immunization of cynomolgus macaque nos. 7–9 with MAP did not elicit cDDR5-specific Abs (Fig. 3*B*). Furthermore, the sera from cynomolgus macaque nos. 11, 13, and 16 at 8 wpim with cDDR5-MAP were also examined by flow cytometry to determine whether they recognize intact cell surface-expressed CCR5 on CEM-CCR5 cells. The sera from no. 11 (diluted 1/5 and 1/100), no. 13 (diluted 1/5 and 1/100), and no. 16 (diluted 1/100 and 1/400) macaques showed the immunofluorescence staining of CEM-CCR5 cells, compared with preimmunization sera from these macaques (Fig. 3, *C–H*). In contrast, the immunization of cynomolgus macaque nos. 7–9 with MAP did not induce CCR5-specific Abs (data not shown).

Inhibition of HIV-1 infection

The anti-HIV-1 activities of the immune sera from cynomolgus macaque nos. 11, 13, and 16 were also determined using MAGIC-5 cells expressing CCR5. The cells were separately inoculated with two laboratory strains of clade B HIV-1 (R5 HIV-1, HIV-1_{JRFL}; X4 HIV-1, HIV-1_{LAV-1}) or R5 nonclade B HIV-1 primary isolates (clade A:$HIV_{93RW004}$ and clade C:HIV_{MJ4}) in the presence or absence of immune sera. As expected, 8 wpim sera from cDDR5-MAP-immunized cynomolgus macaque nos. 11, 13, and 16 markedly suppressed infection by HIV-1_{JRFL} (R5 HIV-1) in a dose-dependent manner (Fig. 4, *D–F*). Furthermore, 10 wpim sera from macaque no. 16 suppressed infection by R5 nonclade B HIV-1 primary isolates (clade A:$HIV_{93RW004}$ and clade C:HIV_{MJ4}) (Fig. 4, *G* and *H*). In contrast, the immune sera did not prevent HIV-1_{LAV-1} (X4 HIV-1) infection as observed in the control experiment (Fig. 4, *A–C*).

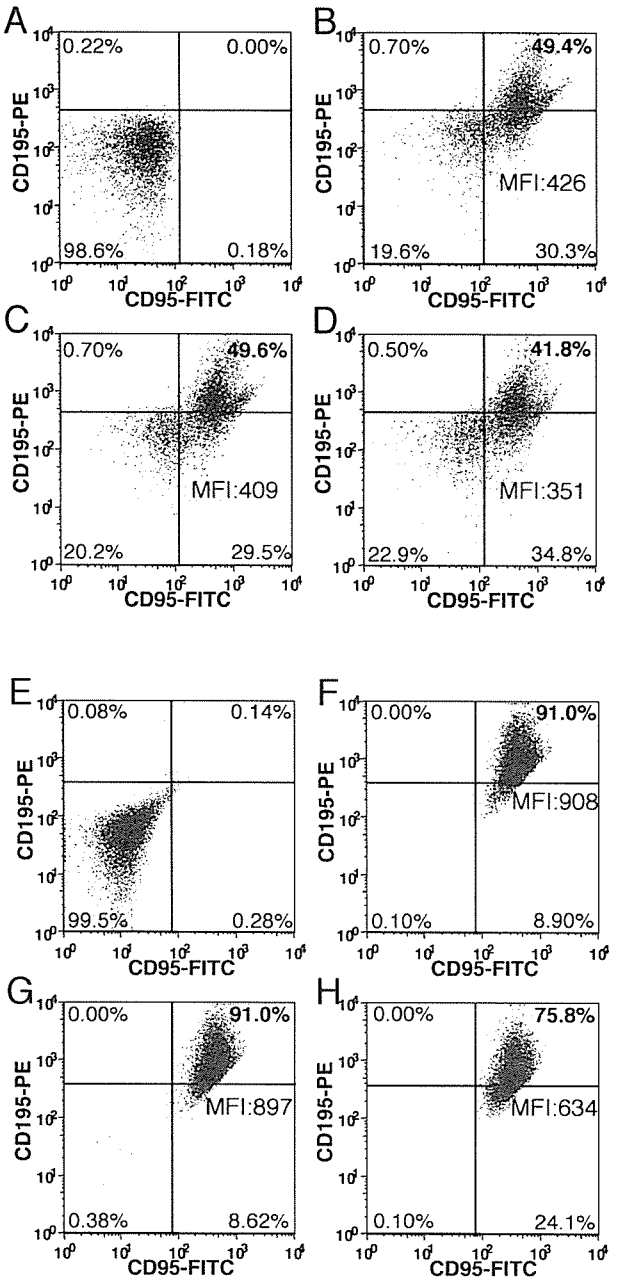

FIGURE 6. Inhibition of binding of a mAb against CCR5 (3A9) to cynomolgus macaque PBMC or HSC-F by anti-cDDR5 serum. Macaque PBMC (*A–D*) or HSC-F (*E–H*) was incubated with FITC-labeled IgG1 and PE-labeled IgG2 (*A* and *E*), FITC-labeled anti-CD95 and PE-labeled anti-human CCR5 mAb (3A9) (*B* and *F*), and FITC-labeled anti-CD95 and PE-labeled anti-human CCR5 mAb (3A9) after preincubation with preimmunization (*C* and *G*) or 10 wpim sera (*D* and *H*). Staining was assessed by flow cytometry, and fluorescence was measured after gating the lymphocyte population. Inhibition of 3A9 binding was determined by two methods: first, by quantitating the percentage of $CD95^+$ cells that were also 3A9-PE positive; second, by determining the mean fluorescence index (MFI) of $CD95^+$ cells that were bound by 3A9. These values are displayed in the quadrant.

Inhibition of CCR5-specific $SHIV_{SF162P3}$ infection

The SHIV-$1_{SF162P3}$ bulk isolate is a pathogenic CCR5-specific SHIV in rhesus macaques (25). The 8 wpim sera from macaque nos. 11, 13, and 16 were examined by infection assay using both MAGIC-5 and CEM-CCR5 cells to determine whether they inhibit SHIV-$1_{SF162P3}$ bulk isolate infection. The 8 wpim sera significantly suppressed the infection of MAGIC-5 cells by the SHIV-$1_{SF162P3}$ bulk isolate, compared with the preimmune sera (Fig. 5, *A–C*). To verify the antiviral activity of immune sera in another experiment, the inhibitory effect of immune sera from cynomolgus macaque nos. 11, 13, and 16 on $SHIV_{SF162P3}$ replication in CEM-CCR5 cells was investigated. CEM-CCR5 cells, a CCR5-transfected human T cell line, were acutely infected with $SHIV_{SF162P3}$ in the presence of preimmunization and 8 wpim sera from cynomolgus macaque nos. 11, 13, and 16, and the spread of infection was then monitored on the basis of the accumulation of p27 Ag in culture supernatants. The 8 wpim sera from macaque nos. 11, 13, and 16 effectively suppressed $SHIV_{SF162P3}$ propagation (Fig. 5, *D–F*).

Ability of macaque anti-cDDR5 sera to bind to macaque CCR5

The UPA sequence in human and macaque CCR5s differs in 1 aa ($Lys^{171}Arg$). Anti-human CCR5 Ab, 2D7, binds to the epitope that includes Lys^{171}, and this binding ability was prevented by the sequence substitution in CCR5 ($Lys^{171}Arg$). To rule out whether anti-cDDR5 serum cross-reacts with native CCR5 as expressed on macaque lymphocytes, we examined the ability of anti-cDDR5 sera to block the binding of a commercially available CCR5-specific mAb (3A9). The 3A9 can bind to macaque CCR5. Cynomolgus macaque PBMC or the lymphocytic cell line HSC-F (23) was incubated with the anti-CD95 Ab with either the preimmunization or 10 wpim serum from cynomolgus macaque no. 16 and then reacted with a limiting amount of PE-labeled 3A9 according to the protocol of Chackerian et al. (13). The ability of anti-cDDR5 serum to block 3A9-PE binding was assessed by flow cytometry, gating lymphocytes, and examining the $CD95^+$ population. The incubation of PBMC or HSC-F with 10 wpim serum reduced the percentage of $CD95^+$ lymphocytes that were 3A9 positive (Fig. 6, *D* and *H*). In addition, the mean fluorescence index of cells that remained 3A9 positive was lower than that of cells that were preincubated with preimmunization serum. The 10 wpim serum did not decrease the binding of a control mAb (anti-CD95-FITC), suggesting that the observed inhibition of 3A9 binding was specific. In addition, the incubation of PBMC or HSC-F with preimmunization serum from macaque no. 16 had no effect on 3A9-PE binding (Fig. 6, *C* and *G*). Taken together, these results support the conclusion that anti-cDDR5 serum cross-reacts with native CCR5 as expressed on macaque lymphocytes.

Macaque challenge with $SHIV_{SF162P3}$

Five weeks after the final boost (11 wpim), all of the MAP- and cDDR5-MAP-immunized macaques were i.v. challenged with 1 ml of 10 $TCID_{50}$/ml $SHIV_{SF162P3}$, which is a chimeric virus that contains the *env*, *tat*, and *rev* genes from HIV_{SF162}, an R5 virus, in the background of SIV_{mac239}. The course of acute viral infection was monitored by measuring plasma viral RNA load and $CD4^+$ T cell number in acutely infected macaques (Fig. 7). All of the three control macaques developed detectable plasma viremia, as demonstrated by viral peaks between 1×10^9 and 3×10^9 viral RNA copies/ml plasma with a moderate decrease in peripheral $CD4^+$ T cell number (%), as previously described (25), and sustained plasma viremia $>10^8$ viral RNA copies/ml plasma for 3 wk (1–4 wk postchallenge). The actual percentage of surviving peripheral $CD4^+$ T cells inversely correlated with viral load (Fig. 7). Furthermore, we compared the geometric mean plasma viral RNA loads of the vaccinated and control groups to monitor the effectiveness of vaccination. The difference between viral loads of the two groups was statistically significant ($p = 0.03$) at one time point (week 1) by 4 wk after infection (Table I), and there were

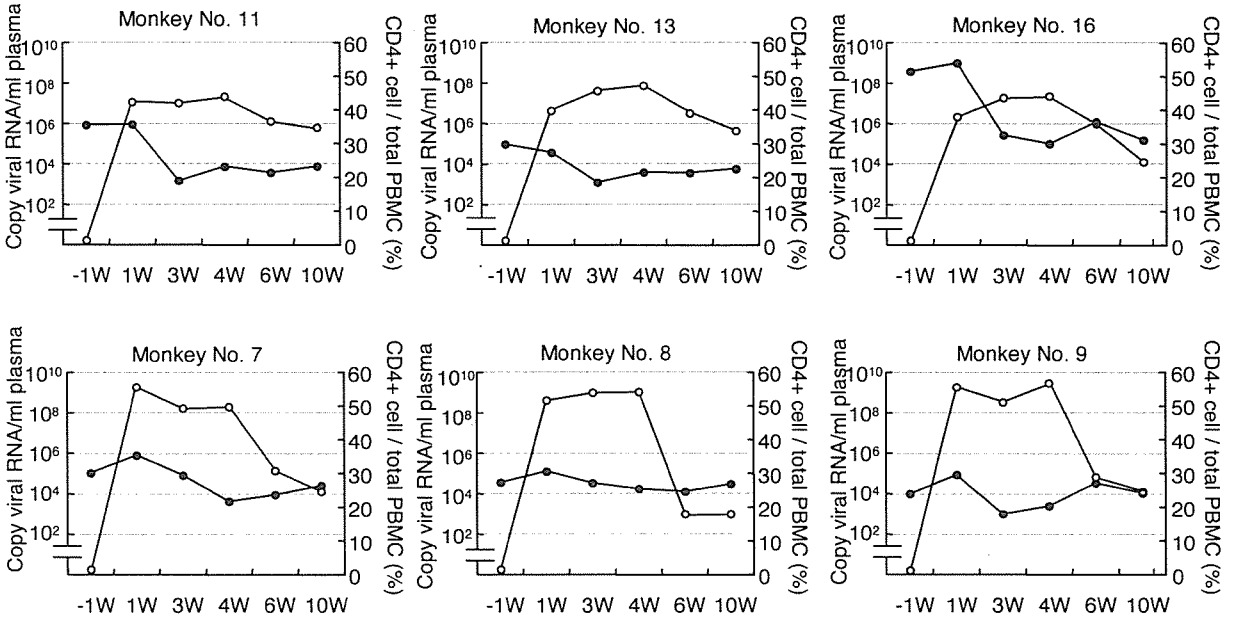

FIGURE 7. Intravenous challenge with $SHIV_{SF162P3}$. Whole-blood samples were collected at −1, 1, 3, 4, 6, and 10 wk postchallenge, and the samples were examined for plasma viremia (○) and peripheral $CD4^+$ T cell count (%) (●). Viral RNA was extracted from macaque plasma and then reverse transcribed. The resulting cDNA duplicates were amplified by quantitative real-time PCR, as described in *Materials and Methods*.

differences of ~19.95- to 217.10-fold in the geometric mean viral loads of the two groups between 1 and 4 wk postchallenge. The vaccinated macaques had a lower ~3-wk delayed peak viremia than the controls, so that the vaccinated macaques sustained plasma viremia between 10^4 and 3×10^6 viral RNA copies/ml plasma at 6 and 10 wk postchallenge in contrast to control macaques (between 10^3 and 10^5 viral RNA copies/ml plasma). Furthermore, we investigated whether the high in vitro anti-HIV and in vitro anti-SHIV activities are associated with low viral loads during the acute phase of SHIV infection. The in vitro anti-HIV and in vitro anti-SHIV activities before challenge were compared with the peak plasma viral RNA load at 1 wk postchallenge (Table II). Macaque no. 16 with the highest anti-HIV and anti-SHIV activities had the lowest viral load among vaccinated macaques at 1 wk postchallenge (2.0×10^6 viral RNA copies/ml plasma), suggesting that the higher in vitro anti-HIV and in vitro anti-SHIV activities in vaccinated macaques were responsible for the low viral loads (Table II). Taken together, these results suggest that viral loads in vaccinated macaques following a challenge with $SHIV_{SF162P3}$ are controlled for a longer time if the anti-CCR5 Ab continues to be strongly induced by vaccination for a longer time.

Table I. *Statistical analysis of geometric mean viral loads*

	Comparison of Geometric Mean Viral Load of Vaccinated Group with That of Control Group	
Postchallenge (wk)	Ratio[a]	*p* Value[b]
1	**217.10**	**0.03**
3	19.95	0.11
4	28.40	0.05
6	0.04	[c]
10	0.02	[c]

[a] The ratio of the geometric mean titers at the indicated time points postchallenge. A value of 217.10 indicates that the geometric mean viral load of the control group is 217.10 times higher than that of the vaccinated group.

[b] Values of *p* were obtained from a two-sample *t* test at the indicated time points. The Mann-Whitney *U* test also provided similar statistical results. Value in boldface is statistically significant ($p < 0.05$).

[c] Value of *p* was not calculated because the geometric mean viral load of the vaccinated group is higher than that of the control group.

Discussion

CCR5 is considered important in HIV-1 transmission on the basis of the findings that individuals homozygous for a 32-bp deletion in the CCR5-coding region have a very low susceptibility to HIV-1 infection (15–18), and CCR5-reactive Abs in ESN subjects downmodulate surface CCR5 in vivo and neutralize the infectivity of R5 strains (21). Therefore, the induction of CCR5-specific autoantibody-based immunity specific to the infection by R5 HIV-1 from various HIV-1 clades may be a strategy for the development of a prophylactic HIV-1 vaccine.

Some vaccination strategies of inducing CCR5-specific autoantibodies have been reported. One of our previous attempts was to induce CCR5-specific autoantibodies with anti-R5 HIV-1 activity by the inoculation of cDDR5-MAP from the UPA (from Arg^{168} to Cys^{178}) of extracellular loop-2 in CCR5 into BALB/c mice (10). Other attempts include the induction of CCR5-specific autoantibodies with anti-R5 HIV-1 activity by the inoculation of recombinant papillomavirus-like particles, which represent an extracellular loop of CCR5, into C57BL/6 mice and pig-tail macaques (12, 13), by the genetic immunization of cynomolgus macaques with the DNA of CCR5 (14), and by the immunization of rhesus macaques with synthetic linear peptides (N-terminal peptide 1–20, first-loop peptide 89–102, and second loop peptide 178–197) derived from the N terminus, first loop, and second loop in CCR5 (11). Results of these previous studies indicate that vaccines aimed at inducing CCR5-specific autoantibodies can be developed, as well as conventional viral protein-based vaccines.

In our present study, a cyclopeptide immunogen strategy was used to induce CCR5-specific autoantibodies in cynomolgus macaques. The advantages of a cyclopeptide immunogen are as follows: 1) it can induce Abs against a very restricted region that includes a biologically active conformational epitope; 2) its immunogenicity can be controlled by polymerization or conjugation with small carrier molecules such as MAP; and 3) its chemical

Table II. *Relationship among anti-cDDR5 Ab response, antiviral activity, and viral load in cynomolgus macaques*

Cynomolgus Macaque	Anti-HIV Activity (IC_{50}, dilution of dialyzed immune sera) at 8 wk Postinitial Immunization[a]	Anti-SHIV Activity (%) at 8 wk Postinitial Immunization[b]	Peak Viral Load at 1 wk Postchallenge[c]
Monkey no. 11	1/40	20	1.0×10^7
Monkey no. 13	1/105	84	4.0×10^6
Monkey no. 16	1/200	91	2.0×10^6
Monkey no. 7	Nd[d]	Nd[d]	2.0×10^9
Monkey no. 8	Nd[d]	Nd[d]	4.0×10^8
Monkey no. 9	Nd[d]	Nd[d]	2.0×10^9

[a] Antiviral activity was determined by MAGIC-5 assay using HIV-1_{JRFL} data shown in Fig. 4, D–F.
[b] Antiviral activity was determined by MAGIC-5 assay using SHIV-$1_{SF162P3}$ data shown in Fig. 5, A–C. Values were calculated using the following equation: 100 − (relative % of control (%)).
[c] Based on data shown in Fig. 7.
[d] Antiviral activity was not detected.

purity can be exactly defined (29, 30). In particular, the conformational stability of a peptide immunogen in vivo is a key factor for generating Abs against a native protein. In general, an Ab induced by a linear peptide can recognize a denatured protein, but not a native protein. In contrast, an Ab that recognizes the conformational epitope of an Ag cannot recognize a denatured protein. Indeed, the commercially available anti-CXCR4 Ab 12G5 can recognize the conformational epitope of cell surface CXCR4, but cannot detect denatured CXCR4. Therefore, cDDR5-MAP was designed on the basis of the deduced conformation of UPA (Arg^{168} to Cys^{178}) in CCR5 to induce Abs that can recognize native CCR5. In addition, the reason for selecting UPA as the target in our study is that the conformational heterogeneity of UPA is unlikely to arise, except for other extracellular domains because cysteine residues (Cys^{101} and Cys^{178}) in extracellular loop-1 and extracellular loop-2 form a rigid disulfide bond. Consequently, cDDR5 was prepared by the cyclization of the decapeptide (R_{168}SQKEGL HYT$_{177}$) derived from the UPA sequence by the insertion of the spacer-armed dipeptide (Gly-Glu). cDDR5 can induce CCR5-specific autoantibodies capable of significantly inhibiting infection by the R5 laboratory-adapted strain (HIV-1_{JRFL}), R5 HIV-1 primary isolates (clade A:$HIV_{93RW004}$ and clade C:HIV_{MJ4}), and $SHIV_{SF162P3}$ bulk isolates (Figs. 4 and 5). These results suggest that UPA in CCR5 is a good target for preventing CCR5-dependent viral infection. Thompson et al. (31) found that in contrast to clade B isolates, a cluster of residues in the second extracellular loop of CCR5 significantly affects the fusion and entry of all the nonclade B isolates tested. Therefore, cDDR5-MAP derived from UPA may be a more useful immunogen than that derived from other domains of CCR5, except UPA as a HIV-1 coreceptor-based vaccine candidate for use in worldwide AIDS epidemics.

To assess vaccine efficiency, we infected the control and cDDR5-MAP-immunized macaques with an R5-tropic $SHIV_{SF162P3}$. All of the three control macaques developed detectable plasma viremia, as demonstrated by viral peaks between 1×10^9 and 3×10^9 viral RNA copies/ml plasma with a moderate decrease in peripheral $CD4^+$ T cell number (%) and sustained plasma viremia $>10^8$ viral RNA copies/ml plasma for 3 wk (1–4 wk postchallenge). Reyes et al. (32) have recently demonstrated that i.v. $SHIV_{SF162P3}$ inoculation moderately decreases the absolute number of peripheral blood $CD4^+$ T cells at 2–3 wk postinfection, as we have observed. In contrast, all of the vaccinated macaques also developed detectable plasma viremia at 1 wk postchallenge, and the plasma viremia levels in the three vaccinated macaques peaked ~3 wk later than those in the control macaques (Fig. 7), so that the vaccinated macaques sustained plasma viremia levels between 10^4 and 3×10^6 viral RNA copies/ml plasma at 6 and 10 wk postchallenge in contrast to the control macaques (between 10^3 and 10^5 viral RNA copies/ml plasma). However, Table I shows there are differences of ~19.95- to 217.10-fold in the geometric mean viral loads of the two groups between 1 and 4 wk postchallenge, and at one time point (week 1), the difference (217.10-fold) was statistically significant ($p = 0.03$). Furthermore, Table II suggests that the higher in vitro anti-HIV and in vitro anti-SHIV activities of anti-cDDR5 sera are responsible for the low viral loads. These results suggest that the high induction of the anti-CCR5 Ab can suppress viral propagation during acute HIV-1 transmission, but only high induction of the anti-CCR5 Ab is not sufficient to clear detectable plasma-associated viruses because the anti-CCR5 Ab does not directly neutralize $SHIV_{SF162P3}$. It seems difficult to completely eliminate or inhibit HIV-1 acute infection in vivo even if only the anti-CCR5 Ab delays viral propagation during the initial HIV-1 transmission. Lopalco et al. (33) have recently reported that antivirus Abs such as IgA to gp41 are simultaneously induced with IgG to CCR5 and IgG to CD4 in some Italian ESN subjects. These humoral immune responses contribute to an extremely low level of viral replication below the detection limit of a standard assay in ESN subjects. Moreover, there is a possibility that more than one type of immunity such as anti-CCR5 and anti-HIV humoral responses must be induced by a vaccine if that vaccine is to be effective for HIV.

In conclusion, immunization with cDDR5-MAP induces CCR5-specific Abs in cynomolgus macaques and decreases viral load at peak viremia. Our results suggest that the CCR5-based cycloimmunogen strategy using cDDR5-MAP induces CCR5-specific autoantibodies capable of inhibiting R5 HIV-1 infection. With the basic knowledge of the induction of CCR5-specific Abs using cDDR5-MAP, we are currently developing cDDR5-MAP conjugated to the HIV env protein to reconstruct the immune response in ESN subjects.

Acknowledgments

We thank Drs. Y. Maeda and S. Harada (Kumamoto University) for providing the CEM-CCR5 cell lines. We also thank Dr. M. Tatsumi (National Institute of Infectious Diseases, Tokyo, Japan) for providing the MAGIC-5 cells. BIAcore analysis was supported by the Center for AIDS Research, Kumamoto University. $HIV_{93RW004}$, HIV_{MJ4}, and $SHIV_{SF162P3}$ were obtained through the AIDS Research and Reference Reagent Program, Division of AIDS, National Institute of Allergy and Infectious Diseases, National Institutes of Health. We thank K. Tokunaga for excellent technical assistance.

Disclosures

The authors have no financial conflict of interest.

References

1. World Health Organization, UNAIDS. 2001. Approaches to the development of broadly protective HIV vaccines: challenges posed by the genetic, biological and antigenic variability of HIV-1: report from a meeting of the WHO-UNAIDS Vaccine Advisory Committee Geneva, 21–23 February 2000. *AIDS* 15: W1–W25.
2. Gaschen, B., J. Taylor, K. Yusim, B. Foley, F. Gao, D. Lang, V. Novitsky, B. Haynes, B. H. Hahn, T. Bhattacharya, and B. Korber. 2002. Diversity considerations in HIV-1 vaccine selection. *Science* 296: 2354–2360.
3. Hanke, T., A. J. McMichael, M. Mwau, E. G. Wee, I. Ceberej, S. Patel, J. Sutton, M. Tomlinson, and R. V. Samuel. 2002. Development of a DNA-MVA/HIVA vaccine for Kenya. *Vaccine* 20: 1995–1998.
4. McMichael, A., M. Mwau, and T. Hanke. 2002. HIV T cell vaccines, the importance of clades. *Vaccine* 20: 1918–1921.
5. Berman, P. W., W. Huang, L. Riddle, A. M. Gray, T. Wrin, J. Vennari, A. Johnson, M. Klaussen, H. Prashad, C. Kohne, et al. 1999. Development of bivalent (B/E) vaccines able to neutralize CCR5-dependent viruses from the United States and Thailand. *Virology* 265: 1–9.
6. Nabel, G., W. Makgoba, and J. Esparza. 2002. HIV-1 diversity and vaccine development. *Science* 296: 2335.
7. Barnett, S. W., S. Lu, I. Srivastava, S. Cherpelis, A. Gettie, J. Blanchard, S. Wang, I. Mboudjeka, L. Leung, Y. Lian, et al. 2001. The ability of an oligomeric human immunodeficiency virus type 1 (HIV-1) envelope antigen to elicit neutralizing antibodies against primary HIV-1 isolates is improved following partial deletion of the second hypervariable region. *J. Virol.* 75: 5526–5540.
8. Chakrabarti, B. K., W. P. Kong, B. Y. Wu, Z. Y. Yang, J. Friborg, X. Ling, S. R. King, D. C. Montefiori, and G. J. Nabel. 2002. Modifications of the human immunodeficiency virus envelope glycoprotein enhance immunogenicity for genetic immunization. *J. Virol.* 76: 5357–5368.
9. Novitsky, V., U. R. Smith, P. Gilbert, M. F. McLane, P. Chigwedere, C. Williamson, T. Ndung'u, I. Klein, S. Y. Chang, T. Peter, et al. 2002. Human immunodeficiency virus type 1 subtype C molecular phylogeny: consensus sequence for an AIDS vaccine design? *J. Virol.* 76: 5435–5451.
10. Misumi, S., R. Nakajima, N. Takamune, and S. Shoji. 2001. A cyclic dodecapeptide-multiple-antigen peptide conjugate from the undecapeptidyl arch (from Arg^{168} to Cys^{178}) of extracellular loop 2 in CCR5 as a novel human immunodeficiency virus type 1 vaccine. *J. Virol.* 75: 11614–11620.
11. Lehner, T., C. Doyle, Y. Wang, K. Babaahmady, T. Whittall, L. Tao, L. Bergmeier, and C. Kelly. 2001. Immunogenicity of the extracellular domains of C-C chemokine receptor 5 and the in vitro effects on simian immunodeficiency virus or HIV infectivity. *J. Immunol.* 166: 7446–7455.
12. Chackerian, B., D. R. Lowy, and J. T. Schiller. 1999. Induction of autoantibodies to mouse CCR5 with recombinant papillomavirus particles. *Proc. Natl. Acad. Sci. USA* 96: 2373–2378.
13. Chackerian, B., L. Briglio, P. S. Albert, D. R. Lowy, and J. T. Schiller. 2004. Induction of autoantibodies to CCR5 in macaques and subsequent effects upon challenge with an R5-tropic simian/human immunodeficiency virus. *J. Virol.* 78: 4037–4047.
14. Zuber, B., J. Hinkula, D. Vodros, P. Lundholm, C. Nilsson, A. Morner, M. Levi, R. Benthin, and B. Wahren. 2000. Induction of immune responses and break of tolerance by DNA against the HIV-1 coreceptor CCR5 but no protection from SIVsm challenge. *Virology* 278: 400–411.
15. Dean, M., M. Carrington, C. Winkler, G. A. Huttley, M. W. Smith, R. Allikmets, J. J. Goedert, S. P. Buchbinder, E. Vittinghoff, E. Gomperts, et al. 1996. Genetic restriction of HIV-1 infection and progression to AIDS by a deletion allele of the CKR5 structural gene: Hemophilia Growth and Development Study, Multicenter AIDS Cohort Study, Multicenter Hemophilia Cohort Study, San Francisco City Cohort, ALIVE Study. *Science* 273: 1856–1862.
16. Huang, Y., W. A. Paxton, S. M. Wolinsky, A. U. Neumann, L. Zhang, T. He, S. Kang, D. Ceradini, Z. Jin, K. Yazdanbakhsh, et al. 1996. The role of a mutant CCR5 allele in HIV-1 transmission and disease progression. *Nat. Med.* 2: 1240–1243.
17. Liu, R., W. A. Paxton, S. Choe, D. Ceradini, S. R. Martin, R. Horuk, M. E. MacDonald, H. Stuhlmann, R. A. Koup, and N. R. Landau. 1996. Homozygous defect in HIV-1 coreceptor accounts for resistance of some multiply exposed individuals to HIV-1 infection. *Cell* 86: 367–377.
18. Samson, M., F. Libert, B. J. Doranz, J. Rucker, C. Liesnard, C. M. Farber, S. Saragosti, C. Lapoumeroulie, J. Cognaux, C. Forceille, et al. 1996. Resistance to HIV-1 infection in Caucasian individuals bearing mutant alleles of the CCR-5 chemokine receptor gene. *Nature* 382: 722–725.
19. Zimmerman, P. A., A. Buckler-White, G. Alkhatib, T. Spalding, J. Kubofcik, C. Combadiere, D. Weissman, O. Cohen, A. Rubbert, G. Lam, et al. 1997. Inherited resistance Chopek, to HIV-1 conferred by an inactivating mutation in CC chemokine receptor 5: studies in populations with contrasting clinical phenotypes, defined racial background, and quantified risk. *Mol. Med.* 3: 23–36.
20. Stewart, G. 1998. Chemokine genes: beating the odds. *Nat. Med.* 4: 275–277.
21. Lopalco, L., C. Barassi, C. Pastori, R. Longhi, S. E. Burastero, G. Tambussi, F. Mazzotta, A. Lazzarin, M. Clerici, and A. G. Siccardi. 2000. CCR5-reactive antibodies in seronegative partners of HIV-seropositive individuals down-modulate surface CCR5 in vivo and neutralize the infectivity of R5 strains of HIV-1 In vitro. *J. Immunol.* 164: 3426–3433.
22. Xu, Y., X. Zhang, M. Matsuoka, and T. Hattori. 2000. The possible involvement of CXCR4 in the inhibition of HIV-1 infection mediated by DP178/gp41. *FEBS Lett.* 487: 185–188.
23. Akari, H., T. Fukumori, S. Iida, and A. Adachi. 1999. Induction of apoptosis in Herpesvirus saimiri-immortalized T lymphocytes by blocking interaction of CD28 with CD80/CD86. *Biochem. Biophys. Res. Commun.* 263: 352–356.
24. Harouse, J. M., A. Gettie, T. Eshetu, R. C. Tan, R. Bohm, J. Blanchard, G. Baskin, and C. Cheng-Mayer. 2001. Mucosal transmission and induction of simian AIDS by CCR5-specific simian/human immunodeficiency virus SHIV(SF162P3). *J. Virol.* 75: 1990–1995.
25. Harouse, J. M., A. Gettie, R. C. Tan, J. Blanchard, and C. Cheng-Mayer. 1999. Distinct pathogenic sequela in rhesus macaques infected with CCR5 or CXCR4 utilizing SHIVs. *Science* 284: 816–819.
26. Gibellini, D., F. Vitone, E. Gori, P. M. La, and M. C. Re. 2004. Quantitative detection of human immunodeficiency virus type 1 (HIV-1) viral load by SYBR green real-time RT-PCR technique in HIV-1 seropositive patients. *J. Virol. Methods* 115: 183–189.
27. Ui, M., T. Kuwata, T. Igarashi, K. Ibuki, Y. Miyazaki, I. L. Kozyrev, Y. Enose, T. Shimada, H. Uesaka, H. Yamamoto, et al. 1999. Protection of macaques against a SHIV with a homologous HIV-1 Env and a pathogenic SHIV-89.6P with a heterologous Env by vaccination with multiple gene-deleted SHIVs. *Virology* 265: 252–263.
28. Palczewski, K., T. Kumasaka, T. Hori, C. A. Behnke, H. Motoshima, B. A. Fox, I. Le Trong, D. C. Teller, T. Okada, R. E. Stenkamp, et al. 2000. Crystal structure of rhodopsin: a G protein-coupled receptor. *Science* 289: 739–745.
29. Arnon, R., and R. J. Horwitz. 1992. Synthetic peptides as vaccines. *Curr. Opin. Immunol.* 4: 449–453.
30. Dakappagari, N. K., D. B. Douglas, P. L. Triozzi, V. C. Stevens, and P. T. Kaumaya. 2000. Prevention of mammary tumors with a chimeric HER-2 B-cell epitope peptide vaccine. *Cancer Res.* 60: 3782–3789.
31. Thompson, D. A., E. G. Cormier, and T. Dragic. 2002. CCR5 and CXCR4 usage by non-clade B human immunodeficiency virus type 1 primary isolates. *J. Virol.* 76: 3059–3064.
32. Reyes, R. A., D. R. Canfield, U. Esser, L. A. Adamson, C. R. Brown, C. Cheng-Mayer, M. B. Gardner, J. M. Harouse, and P. A. Luciw. 2004. Induction of simian AIDS in infant rhesus macaques infected with CCR5- or CXCR4-utilizing simian-human immunodeficiency viruses is associated with distinct lesions of the thymus. *J. Virol.* 78: 2121–2130.
33. Lopalco, L., C. Barassi, C. Paolucci, D. Breda, D. Brunelli, M. Nguyen, J. Nouhin, T. T. Luong, L. X. Truong, M. Clerici, et al. 2005. Predictive value of anti-cell and anti-human immunodeficiency virus (HIV) humoral responses in HIV-1-exposed seronegative cohorts of European and Asian origin. *J. Gen. Virol.* 86: 339–348.

Brief Articles

Identification of a New Class of Low Molecular Weight Antagonists against the Chemokine Receptor CXCR4 Having the Dipicolylamine−Zinc(II) Complex Structure

Hirokazu Tamamura,*,† Akio Ojida,‡ Teppei Ogawa,§ Hiroshi Tsutsumi,† Hiroyuki Masuno,† Hideki Nakashima,∥ Naoki Yamamoto,⊥ Itaru Hamachi,‡ and Nobutaka Fujii*,§

Institute of Biomaterials and Bioengineering, Tokyo Medical and Dental University, Chiyoda-ku, Tokyo 101-0062, Japan, Graduate School of Engineering, Kyoto University, Nishikyo-ku, Kyoto 615-8510, Japan, Graduate School of Pharmaceutical Sciences, Kyoto University, Sakyo-ku, Kyoto 606-8501, Japan, School of Medicine, St. Marianna University, Miyamae-ku, Kawasaki 216-8511, Japan, and AIDS Research Center, National Institute of Infectious Diseases, Shinjuku-ku, Tokyo 162-8640, Japan

Received January 10, 2006

Several low molecular weight nonpeptide compounds having the dipicolylamine−zinc(II) complex structure were identified as potent and selective antagonists of the chemokine receptor CXCR4. These compounds showed strong inhibitory activity against CXCL12 binding to CXCR4, and the top compound exhibited significant anti-HIV activity. Zinc(II)−dipicolylamine unit-containing compounds proved to be useful and attractive lead compounds for chemotherapy of these diseases as nonpeptide CXCR4 antagonists possessing the novel scaffold structure.

Introduction

CXCR4 is a chemokine receptor that transduces signals of its endogenous ligand, CXCL12/stromal cell-derived factor-1 (SDF-1).[1−4] CXCR4 is classified into 7TMGPCR and plays a physiologically critical role by the action of CXCL12 in the migration of progenitors during embryologic development of the cardiovascular, hemopoietic, central nervous systems, etc. In addition, CXCR4 was previously identified as a coreceptor that is used by X4-HIV-1 in its entry into T cells[5] and has recently been proven to be involved in several problematic diseases, including HIV infection, metastasis of several types of cancer,[6−8] leukemia cell progression,[9,10] rheumatoid arthritis (RA).[11,12] Thus, CXCR4 is thought to be a great therapeutic target to overcome these diseases, and several inhibitors directed against CXCR4 have been developed to date.[13−22] We previously found a highly potent CXCR4 antagonist, T140, which is a 14-mer peptide with a disulfide bridge, and its downsized derivative, FC131, which has a cyclic pentapeptide scaffold structure (Table 1).[18−21] Although reduction of the peptide character based on these peptides is underway,[23,24] we would like to discover novel CXCR4 antagonists having nonpeptide structures, since few nonpeptide compounds with low molecular weight have been reported, such as AMD3100 series[14,16] and KRH-1636.[22] Previously, anthracene derivatives having two sets of zinc(II)−2,2′-dipicolylamine (Dpa) complex were identified as the first chemosensors that can selectively bind and sense phosphorylated peptide surfaces.[25] In the present study, we have found several aromatic compounds having the zinc(II)−Dpa structure to be a new class of low molecular weight CXCR4 antagonists.

* Corresponding authors. H.T.: tel. +81 3 5280 8036; fax, +81 3 5280 8039; e-mail. tamamura.mr@tmd.ac.jp. N.F.: tel. +81 75 753 4551; fax. +81 75 753 4570; e-mail. nfujii@pharm.kyoto-u.ac.jp.

† Tokyo Medical and Dental University.

‡ Graduate School of Engineering, Kyoto University.

§ Graduate School of Pharmaceutical Sciences, Kyoto University.

∥ St. Marianna University.

⊥ National Institute of Infectious Diseases.

Experimental Section

Chemistry. Synthesis of Bis(dipicolylamine)-*p*-xylene−Zn Complexes. Aromatic compounds having the zinc(II)−Dpa structure were previously synthesized as reported elsewhere.[25−28]

For a comparative study, bis(3,3′- and bis(4,4′-dipicolylamine)-*p*-xylenes, **24** and **25**, respectively, were synthesized by treatment of *p*-xylenediamine with the corresponding pyridinecarbaldehydes and sodium triacetoxyborohydride [$NaBH(OAc)_3$] (Figure 1).[29] Zinc(II) complexation in the preparation of **18** and **19** was performed by treatment of bis(dipicolylamine)-*p*-xylenes with NaOH to afford salt-free compounds, followed by addition of aqueous zinc nitrate [$Zn(NO_3)_2$].

Biological Assays. Calcium mobilization,[30] [^{125}I]CXCL12 binding (oil cushion method),[30] and anti-HIV[23] assays were performed as reported previously.

Molecular Modeling Calculations. Molecular modeling calculations were performed using SYBYL program (version 7.0, TRIPOS Inc.). Energy minimizations were performed using Tripos force field. The lowest energy conformation was obtained by random search method.

Biological Results and Discussion

Several aromatic compounds having the zinc(II)−dipicolylamine structure were prepared and surveyed for CXCR4-antagonistic activity based on inhibitory activity against Ca^{2+} mobilization induced by CXCL12 stimulation through CXCR4. The structures and CXCR4-antagonistic activity of these compounds are shown in Tables 1−3. Positive controls **8** (T140), **9** (FC131), and **10** (KRH-1636) showed strong antagonistic activity. Compound **2**, which has two sets of the [bis(pyridin-2-ylmethyl)amino]methylene unit with zinc(II) complexation at the para-position of benzene, showed potent CXCR4-antagonistic activity ($IC_{50} = 0.1\ \mu M$). Compound **1**, which has a piece of this unit, did not show any activity until 1 μM. It suggests that two sets of this unit are required for binding to CXCR4. Compound **3**, which has two sets of this unit at the meta-position of benzene, showed lower activity than compound **2**, suggesting that the presence of this unit at the para-position is critical for

10.1021/jm060025u CCC: $33.50
Published on Web 05/03/2006

Table 1. Structures and CXCR4-Antagonistic Activity of Aromatic Compounds Having the Zinc(II)−Dipicolylamine Structure (I)

Compd. (No.)	Structure	IC_{50} (μM)[a]
1	Zn·Dpa; Dpa·Zn = 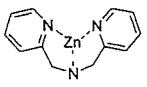	> 1
2	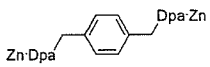	0.10
3	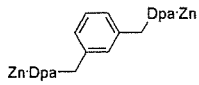	0.49
4	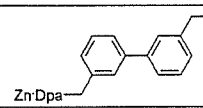	0.35
5	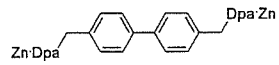	0.12
6	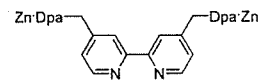	0.46
7	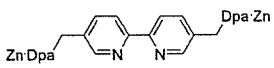	0.10
8	H-Arg-Arg-Nal-Cys-Tyr-Arg-Lys-D-Lys-Pro-Tyr-Arg-Cit-Cys-Arg-OH T140	0.0036
9	*cyclo*(-Nal-Gly-D-Tyr-Arg-Arg-) FC131	0.036
10	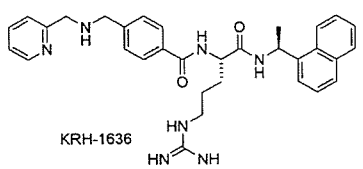 KRH-1636	0.040

[a] IC_{50} values are based on the inhibition against Ca^{2+} mobilization induced by CXCL12 stimulation through CXCR4. All data are the mean values for at least two independent experiments.

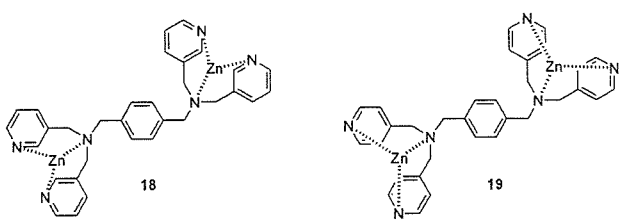

Figure 1. Structures of the zinc(II)−bis(3,3′- and −bis(4,4′-dipicolylamine)-*p*-xylene (**24** and **25**) complexes, **18** and **19**, respectively.

strong CXCR4-antagonistic activity. Biphenyl compounds having two sets of this unit at the 3,3′- and 4,4′-positions, **4** and **5**, respectively, exhibited significantly high antagonistic activity, although the compound with the 4,4′-positions substituted (**5**) is stronger than that having the 3,3′-positions substituted (**4**). It seems to be important that two sets of the [bis(pyridin-2-ylmethyl)amino]methylene unit with zinc(II) complexation are

Table 2. Structures and CXCR4-Antagonistic Activity of Aromatic Compounds Having the Zinc(II)−Dipicolylamine Structure (II)

Compd. (No.)	Structure	IC_{50} (μM)
11	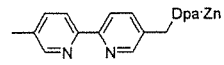	> 1
12	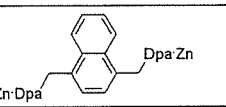	0.18
13	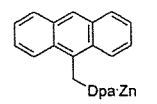	0.77
14	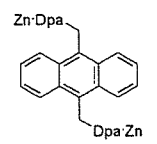	0.24
15	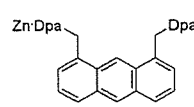	0.75
16	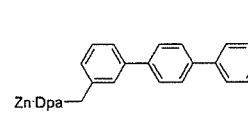	> 1
17	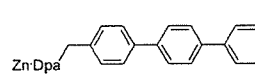	> 1

Table 3. Structures and CXCR4-Antagonistic Activity of Aromatic Compounds Having the Zinc(II)−Dipicolylamine Structure and Zinc-Free Compounds

compd	structure	IC_{50} (μM)
18	shown in Figure 1	> 10
19	shown in Figure 1	> 10
20	zinc-free analogue of **2**	> 10
21	zinc-free analogue of **5**	> 10
22	zinc-free analogue of **7**	> 10
23	zinc-free analogue of **14**	> 10
24	zinc-free analogue of **18**	> 10
25	zinc-free analogue of **19**	> 10

located at 180° of each other as in compounds **2** and **5**, which both have almost the same potency. Furthermore, replacement of the biphenyl unit of compounds **4** and **5** by [2,2′]bipyridinyl did not cause significant change in CXCR4-antagonistic activity, since the [2,2′]bipyridinyl compounds **6** and **7** showed almost the same potency as the biphenyl compounds **4** and **5**, respectively. It may be a matter of course that a [2,2′]bipyridinyl compound having only one [bis(pyridin-2-ylmethyl)amino]-methylene unit with zinc(II) complexation (**11**) did not show any activity until 1 μM, as compound **1** did not. A naphthyl compound (**12**) and an anthracenyl compound (**14**), which have two sets of this unit at the 1,4-positions and at the 9,10-positions,

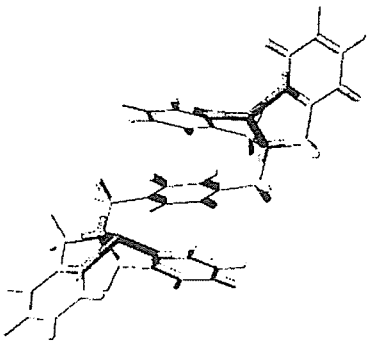

Figure 2. The structure calculated by molecular modeling of compound **2** having the zinc(II)−Dpa structure. Nitrogen atoms, blue; hydrogen atoms, sky blue; zinc atoms, red.

respectively, showed high activity. However, it suggests that the addition of one and two benzene moieties to compound **2** caused a slight decrease in activity. Unexpectedly, an anthracenyl compound having only one [bis(pyridin-2-ylmethyl)-amino]methylene unit with zinc(II) complexation (**13**) exhibited not so high but significant antagonistic activity. It may be reasonable that the anthracenyl compound **15**, which has two sets of this unit at the 1,8-positions, did not show high antagonistic activity, since it is thought to be important that these units are located 180° from each other. In addition, terphenyl compounds **16** and **17** did not show any significant activity until 1 μM, suggesting that it might be unsuitable that two sets of this unit be located far apart from each other.

Next, to investigate whether the location of the nitrogen atom in the pyridine ring of the [bis(pyridin-2-ylmethyl)amino]-methylene unit is critical for expression of CXCR4-antagonistic activity, compounds **18** and **19**, which contained the [bis(pyridin-3-ylmethyl)amino]methylene and [bis(pyridin-4-ylmethyl)amino]methylene units, respectively, with zinc(II) complexation, were synthesized. Neither compound **18** nor **19** showed any significant activity, although antagonistic activity was estimated to 10 μM. This result suggested that the location of the nitrogen atom in the pyridine ring is important either for formation of active conformation or for stable complexation with zinc(II).

Molecular modeling simulation analysis showed that the bis-(3,3′-dipicolylamine) and bis(4,4′-dipicolylamine)-*p*-xylene Zn complexes **18** and **19** did not converge as well as bis(Dpa)−Zn complex **2** did (Figure 2). Values of the coordinate bond lengths between zinc and nitrogen atoms (of the pyridine rings/of the tertiary amine) in the bis(Dpa)−Zn complex **2** are 1.93−1.95 Å, according to molecular modeling calculations. Complex **2** forms a stable conformation, having $\pi-\pi$ stacking among three aromatic rings, as shown in Figure 2. However, values of bond lengths between zinc and nitrogen atoms of the pyridine rings in the complexes **18** and **19** would be ca. 2.9 and ca. 4.2 Å, respectively, which are relatively long. In addition, the proton atoms at the positions 2 and 2′ in the pyridine rings might interfere with the zinc atom to prevent the molecules from forming a stable coordinate conformation.

Furthermore, to verify the indispensability of zinc(II) complexation, zinc-free analogues of **2**, **5**, **7**,and **14**, compounds **20**−**23**, respectively, were assessed for CXCR4-antagonistic activity. Since these zinc-free compounds did not show any significant activity until 10 μM, zinc(II) atoms or conformation constrained by zinc(II) complexation might be indispensable for binding to CXCR4. As a matter of course, zinc-free analogues of **18** and **19**, compounds **24** and **25**, respectively, did not show any significant activity.

Table 4. CXCR4-Binding Activity of Compounds **2**, **5**, **7**, and **12**

compd	IC_{50} (μM)[a]	compd	IC_{50} (μM)[a]
2	0.047	**8** (T140)	0.00093
5	0.18	**9** (FC131)	0.0030
7	0.22	**10** (KRH-1636)	0.034
12	0.42		

[a] IC_{50} values are based on the inhibition of [^{125}I]CXCL12 binding to CXCR4 transfectants of CHO cells. All data are the mean values for at least two independent experiments.

Next, we investigated CXCR4-binding activity of the novel compounds that possess strong CXCR4-antagonistic activity (Table 4). Compounds **2**, **5**, **7**, and **12** showed potent binding activity. Especially, the potency of compound **2** is comparable to that of KRH-1636.

The best and simple compound among the present compounds (**2**) was evaluated for anti-HIV activity. Compound **2** showed significant inhibitory activity against X4-HIV-1-induced cytopathogenicity in MT-4 cells (EC_{50} = 7.1 μM), although anti-HIV activity in cells is lower than CXCR4-antagonistic or -binding activity as usual.[23] Furthermore, the present compounds identified as CXCR4 antagonists showed no significant inhibition (<25%) at 10 μM against Ca^{2+} mobilization induced by MIP-1α stimulation through CCR5 and at 30 μM against Ca^{2+} mobilization induced by sphingosine 1-phosphate stimulation through EDG3 (GPCR).

The present compounds, such as **2**, **5**, **7**, and **12**, have been prepared as binuclear zinc complexes for the use in several assays. The extracellular concentration of zinc is normally ~100 μg/100 mL (approximately 15 μM): 30% of the total zinc is tightly bound to the metal-binding proteins. The remaining amount (70%) is loosely bound to proteins and easily released from the corresponding proteins.[31] Thus, the extracellular concentration of zinc is sufficiently high for the compounds to be active in vivo. Furthermore, the dipicolylamine (Dpa) unit forms a stable complex with zinc ion (log K = 7.57), indicating that the compounds can maintain an active state as the zinc complex in vivo. The affinity of the Dpa unit for Ca^{2+} and Mg^{2+} ions, which are biologically essential, is considerably low (log K < 3). Thus, it is thought that these ions might not affect the zinc complexes.

Conclusion

The current study presents a new class of nonpeptide CXCR4 antagonists with low molecular weight that have a novel scaffold: a dipicolylamine−zinc(II) complex structure. These compounds showed selective and strong CXCR4-antagonistic activity. These compounds also have basic and aromatic moieties in common with several reported CXCR4 antagonists, e.g., T140, FC131, AMD3100 and KRH-1636, suggesting that these moieties are critical for interaction with CXCR4. The present results provide useful insights for the future design of new CXCR4 antagonists in association with information from other CXCR4 antagonists for development of therapeutic strategies for CXCR4-relevant diseases. Furthermore, anthracene derivatives having two sets of zinc(II)−dipicolylamine, such as compound **14**, might be used as chemical probes to study the biology of CXCR4, as these compounds are used to sense phosphorylated peptide surfaces.

Acknowledgment. This work was supported in part by a 21st Century COE Program "Knowledge Information Infrastructure for Genome Science", a Grant-in-Aid for Scientific Research from the Ministry of Education, Culture, Sports, Science and Technology, Japan, and the Japan Health Science Foundation.

Supporting Information Available: Additional experimental procedures of novel synthetic compounds. This material is available free of charge via the Internet at http://pubs.acs.org.

References

(1) Nagasawa, T.; Kikutani, H.; Kishimoto, T. Molecular cloning and structure of a pre-B-cell growth-stimulating factor. *Proc. Natl. Acad. Sci. U.S.A.* **1994**, *91*, 2305−2309.

(2) Bleul, C. C.; Farzan, M.; Choe, H.; Parolin, C.; Clark-Lewis, I.; Sodroski, J.; Springer, T. A. The lymphocyte chemoattractant SDF-1 is a ligand for LESTR/fusin and blocks HIV-1 entry. *Nature* **1996**, *382*, 829−833.

(3) Oberlin, E.; Amara, A.; Bachelerie, F.; Bessia, C.; Virelizier, J.-L.; Arenzana-Seisdedos, F.; Schwartz, O.; Heard, J.-M.; Clark-Lewis, I.; Legler, D. F.; Loetscher, M.; Baggiolini, M.; Moser, B. The CXC chemokine SDF-1 is the ligand for LESTR/fusin and prevents infection by T-cell-line-adapted HIV-1. *Nature* **1996**, *382*, 833−835.

(4) Tashiro, K.; Tada, H.; Heilker, R.; Shirozu, M.; Nakano, T.; Honjo, T. Signal sequence trap: A cloning strategy for secreted proteins and type I membrane proteins. *Science* **1993**, *261*, 600−603.

(5) Feng, Y.; Broder, C. C.; Kennedy, P. E.; Berger, E. A. HIV-1 entry co-factor: Functional cDNA cloning of a seven-transmembrane, G protein-coupled receptor. *Science* **1996**, *272*, 872−877.

(6) Koshiba, T.; Hosotani, R.; Miyamoto, Y.; Ida, J.; Tsuji, S.; Nakajima, S.; Kawaguchi, M.; Kobayashi, H.; Doi, R.; Hori, T.; Fujii, N.; Imamura, M. Expression of stromal cell-derived factor 1 and CXCR4 ligand receptor system in pancreatic cancer: A possible role for tumor progression. *Clin. Cancer. Res.* **2000**, *6*, 3530−3535.

(7) Müller, A.; Homey, B.; Soto, H.; Ge, N.; Catron, D.; Buchanan, M. E.; McClanahan, T.; Murphy, E.; Yuan, W.; Wagner, S. N.; Barrera, J. L.; Mohar, A.; Verastegui, E.; Zlotnik, A. Involvement of chemokine receptors in breast cancer metastasis. *Nature* **2001**, *410*, 50−56.

(8) Tamamura, H.; Hori, A.; Kanzaki, N.; Hiramatsu, K.; Mizumoto, M.; Nakashima, H.; Yamamoto, N.; Otaka, A.; Fujii, N. T140 analogs as CXCR4 antagonists identified as anti-metastatic agents in the treatment of breast cancer. *FEBS Lett.* **2003**, *550*, 79−83.

(9) Tsukada, N.; Burger, J. A.; Zvaifler, N. J.; Kipps, T. J. Distinctive features of "nurselike" cells that differentiate in the context of chronic lymphocytic leukemia. *Blood* **2002**, *99*, 1030−1037.

(10) Juarez, J.; Bradstock, K. F.; Gottlieb, D. J.; Bendall, L. J. Effects of inhibitors of the chemokine receptor CXCR4 on acute lymphoblastic leukemia cells in vitro. *Leukemia* **2003**, *17*, 1294−1300.

(11) Nanki, T.; Hayashida, K.; EI−Gabalawy, H. S.; Suson, S.; Shi, K.; Girschick, H. J.; Yavuz, S.; Lipsky, P. E. Stromal cell-derived factor-1-CXC chemokine receptor interactions play a central role in $CD4^+$ T cell accumulation in rheumatoid arthritis synovium. *J. Immunol.* **2000**, *165*, 6590−6598.

(12) Tamamura, H.; Fujisawa, M.; Hiramatsu, K.; Mizumoto, M.; Nakashima, H.; Yamamoto, N.; Otaka, A.; Fujii, N. Identification of a CXCR4 antagonist, a T140 analog, as an anti-rheumatoid arthritis agent. *FEBS Lett.* **2004**, *569*, 99−104.

(13) Murakami, T.; Nakajima, T.; Koyanagi, Y.; Tachibana, K.; Fujii, N.; Tamamura, H.; Yoshida, N.; Waki, M.; Matsumoto, A.; Yoshie, O.; Kishimoto, T.; Yamamoto, N.; Nagasawa, T. A small molecule CXCR4 inhibitor that blocks T cell line-tropic HIV-1 infection. *J. Exp. Med.* **1997**, *186*, 1389−1393.

(14) Schols, D.; Struyf, S.; Van Damme, J.; Este, J. A.; Henson, G.; De Clercq, E. Inhibition of T-tropic HIV strains by selective antagonization of the chemokine receptor CXCR4. *J. Exp. Med.* **1997**, *186*, 1383−1388.

(15) Doranz, B. J.; Grovit-Ferbas, K.; Sharron, M. P.; Mao, S.-H.; Bidwell Goetz, M.; Daar, E. S.; Doms, R. W.; O'Brien, W. A. A small-molecule inhibitor directed against the chemokine receptor CXCR4 prevents its use as an HIV-1 coreceptor. *J. Exp. Med.* **1997**, *186*, 1395−1400.

(16) Donzella, G. A.; Schols, D.; Lin, S. W.; Este J. A.; Nagashima, K. A.; Maddon, P. J.; Allaway, G. P.; Sakmar, T. P.; Henson, G.; De Clercq, E.; Moore, J. P. AMD3100, a small molecule inhibitor of HIV-1 entry via the CXCR4 co-receptor. *Nat. Med.* **1998**, *4*, 72−77.

(17) Howard, O. M. Z.; Oppenheim, J. J.; Hollingshead, M. G.; Covey, J. M.; Bigelow, J.; McCormack, J. J.; Buckheit, R. W., Jr.; Clanton, D. J.; Turpin, J. A.; Rice, W. G. Inhibition of in vitro and in vivo HIV replication by a distamycin analogue that interferes with chemokine receptor function: A candidate for chemotherapeutic and microbicidal application. *J. Med. Chem.* **1998**, *41*, 2184−2193.

(18) Tamamura, H.; Xu, Y.; Hattori, T.; Zhang, X.; Arakaki, R.; Kanbara, K.; Omagari, A.; Otaka, A.; Ibuka, T.; Yamamoto, N.; Nakashima, H.; Fujii, N. A low molecular weight inhibitor against the chemokine receptor CXCR4: A strong anti-HIV peptide T140. *Biochem. Biophys. Res. Commun.* **1998**, *253*, 877−882.

(19) Tamamura, H.; Omagari, A.; Oishi, S.; Kanamoto, T.; Yamamoto, N.; Peiper, S. C.; Nakashima, H.; Otaka, A.; Fujii, N. Pharmacophore identification of a specific CXCR4 inhibitor, T140, leads to development of effective anti-HIV agents with very high selectivity indexes. *Bioorg. Med. Chem. Lett.* **2000**, *10*, 2633−2637.

(20) Fujii, N.; Oishi, S.; Hiramatsu, K.; Araki, T.; Ueda, S.; Tamamura, H.; Otaka, A.; Kusano, S.; Terakubo, S.; Nakashima, H.; Broach, J. A.; Trent, J. O.; Wang, Z.; Peiper, S. C. Molecular-size reduction of a potent CXCR4-chemokine antagonist using orthogonal combination of conformation- and sequence-based libraries. *Angew. Chem., Int. Ed.* **2003**, *42*, 3251−3253.

(21) Tamamura, H.; Fujii, N. Two Orthogonal Approaches to Overcome Multi-Drug Resistant HIV-1s: Development of Protease Inhibitors and Entry Inhibitors Based on CXCR4 Antagonists. *Curr. Drug Targets*—Infectious Disorders **2004**, *4*, 103−110.

(22) Ichiyama, K.; Yokoyama-Kumakura, S.; Tanaka, Y.; Tanaka, R.; Hirose, K.; Bannai, K.; Edamatsu, T.; Yanaka, M.; Niitani, Y.; Miyano-Kurosaki, N.; Takaku, H.; Koyanagi, Y.; Yamamoto, N. A duodenally absorbable CXC chemokine receptor 4 antagonist, KRH-1636, exhibits a potent and selective anti-HIV-1 activity. *Proc. Natl. Acad. Sci. U.S.A.* **2003**, *100*, 4185−4190.

(23) Tamamura, H.; Hiramatsu, K.; Ueda, S.; Wang, Z.; Kusano, S.; Terakubo, S.; Trent, J. O.; Peiper, S. C.; Yamamoto, N.; Nakashima, H.; Otaka, A.; Fujii, N. Stereoselective synthesis of [L-Arg,L/D-3-(2-naphthyl)alanine]-type (*E*)-alkene dipeptide isosteres and its application to the synthesis and biological evaluation of pseudopeptide analogs of the CXCR4 antagonist FC131. *J. Med. Chem.* **2005**, *48*, 380−391.

(24) Tamamura, H.; Araki, T.; Ueda, S.; Wang, Z.; Oishi, S.; Esaka, A.; Trent, J. O.; Nakashima, H.; Yamamoto, N.; Peiper, S. C.; Otaka, A.; Fujii, N. Identification of novel low molecular weight CXCR4 antagonists by structural tuning of cyclic tetrapeptide-scaffolds. *J. Med. Chem.* **2005**, *48*, 3280−3289.

(25) Ojida, A.; Mito-oka, Y.; Inoue, M.; Hamachi, I. First artificial receptors and chemosensors toward phosphorylated peptide in aqueous solution. *J. Am. Chem. Soc.* **2002**, *124*, 6256−6258.

(26) Mito-oka, Y.; Tsukiji, S.; Hiraoka, T.; Kasagi, N.; Shinkai, S.; Hamachi, I. Zn(II) dipicolylamine-based artificial receptor as a new entry for surface recognition of α-helical peptides in aqueous solution. *Tetrahedron Lett.* **2001**, *42*, 7059−7062.

(27) Ojida, A.; Inoue, M.; Mito-oka, Y.; Hamachi, I. Cross-linking strategy for molecular recognition and fluorescent sensing of a multi-phosphorylated peptide in aqueous solution. *J. Am. Chem. Soc.* **2003**, *125*, 10184−10185.

(28) Ojida, A.; Mito-oka, Y.; Sada, K.; Hamachi, I. Molecular recognition and fluorescence sensing of monophosphorylated peptides in aqueous solution by bis(zinc(II)-dipicolylamine)-based artificial receptors. *J. Am. Chem. Soc.* **2004**, *126*, 2454−2463.

(29) Abdel-Magid, A. F.; Maryanoff, C. A.; Carson, K. G. Reductive amination of aldehydes and ketones by using sodium triacetoxyborohydride. *Tetrahedron Lett.* **1990**, *31*, 5595−5598.

(30) Tamamura, H.; Hiramatsu, K.; Kusano, S.; Terakubo, S.; Yamamoto, N.; Trent, J. O.; Wang, Z.; Peiper, S. C.; Nakashima, H.; Otaka, A.; Fujii, N. Synthesis of potent CXCR4 inhibitors possessing low cytotoxicity and improved biostability based on T140 derivatives. *Org. Biomol. Chem.* **2003**, *1*, 3656−3662.

(31) Vallee, B. L.; Falchuk, K. H. The biochemical basis of zinc physiology. *Phys. Rev.* **1993**, *73*, 79−118.

JM060025U

Available online at www.sciencedirect.com
SCIENCE DIRECT
ELSEVIER
Microbes and Infection 8 (2006) 1539–1549
Microbes and Infection
www.elsevier.com/locate/micinf

Original article

Impaired T-cell differentiation in the thymus at the early stages of acute pathogenic chimeric simian–human immunodeficiency virus (SHIV) infection in contrast to less pathogenic SHIV infection

Makiko Motohara [a], Kentaro Ibuki [a], Ariko Miyake [a], Yoshinori Fukazawa [a], Katsuhisa Inaba [a], Hajime Suzuki [a], Kyoko Masuda [b,c], Nagahiro Minato [b], Hiroshi Kawamoto [c], Tadashi Nakasone [d], Mitsuo Honda [d], Masanori Hayami [a], Tomoyuki Miura [a,*]

[a] *Laboratory of Primate Model, Experimental Research Center for Infectious Diseases, Institute for Virus Research, Kyoto University, 53 Shogoinkawara-Machi, Sakyo-Ku, Kyoto 606-8507, Japan*
[b] *Graduate School of Biostudies, Kyoto University, Japan*
[c] *RIKEN Research Center for Allergy and Immunology, Japan*
[d] *National Institute of Infectious Diseases, Japan*

Received 18 September 2005; accepted 16 January 2006
Available online 21 April 2006

Abstract

One of the mechanisms by which HIV infection induces the depletion of $CD4^+$ T cells has been suggested to be impairment of T-cell development in the thymus, although there is no direct evidence that this occurs. To examine this possibility, we compared T-cell maturation in the intrathymic progenitors between macaques infected with an acute pathogenic chimeric simian–human immunodeficiency virus (SHIV), which causes profound and irreversible $CD4^+$ T-cell depletion, and macaques infected with a less pathogenic SHIV, which causes only a transient $CD4^+$ T-cell decline. Within 27 days post-inoculation (dpi), the two virus infections caused similar increases in plasma viral loads and similar decreases in $CD4^+$ T-cell counts. However, in the thymus, the acute pathogenic SHIV resulted in increased thymic involution, atrophy and the depletion of immature T cells including $CD4^+CD8^+$ double-positive (DP) cells, whereas the less pathogenic SHIV did not have these effects. Ex vivo differentiation of CD3 CD4 CD8 triple-negative (TN) intrathymic progenitors to DP cells was assessed by a monkey–mouse xenogeneic fetal thymus organ culture system. Differentiation was impaired in the TN intrathymic progenitors of the acute pathogenic SHIV-infected monkeys, while differentiation was not impaired in the TN intrathymic progenitors of the less pathogenic SHIV-infected monkeys. These differences suggest that dysfunction of thymic maturation makes an important contribution to the irreversible depletion of circulating $CD4^+$ T cells in vivo.

Keywords: AIDS; Animal model; Rhesus monkey; SHIV; Thymopoiesis

1. Introduction

The mechanisms that contribute to the depletion of circulating $CD4^+$ T lymphocytes in AIDS patients are not completely defined. Multiple mechanisms appear to be involved, including direct destruction of peripheral mature T cells by virus infection and decreased thymic output of mature T cells to the peripheral circulation [1]. HIV infection of the thymus is considered to contribute to the depletion of $CD4^+$ T cells and the development of AIDS [1–3]. The thymus, a major target of HIV infection, is responsible for de novo production of $CD4^+$ and $CD8^+$ T cells from CD3 CD4 CD8 triple-negative (TN) intrathymic progenitors through $CD4^+CD8^+$ double-positive (DP) cells, and therefore is essential for T-cell renewal. In adults, the importance of a functional thymus is not clear. However, the thymus is considered to be critical in

* Corresponding author. Tel.: +81 75 751 3984; fax: +81 75 761 9335.
E-mail address: tmiura@virus.kyoto-u.ac.jp (T. Miura).

1286-4579/$ - see front matter
doi:10.1016/j.micinf.2006.01.011

HIV disease, in which T cells are depleted in large numbers. In fact, histopathological and morphological evidence of thymic dysfunction was found in infants who had experienced rapid onset of severe AIDS [4]. Not only mature T cells but also T-cell progenitors have long been hypothesized to be a target of HIV. The effects of HIV infection on T-cell progenitors have been suggested to limit the potential for compensatory immune cell production [1,5]. However, detailed studies using the organs of HIV-1-infected humans are extremely limited, especially for subjects at the early phase of infection.

Simian immunodeficiency virus (SIV)-induced disease in macaques has contributed to understanding the pathogenesis of AIDS [6,7]. Nevertheless, because SIV is genetically similar to, but not the same as, HIV, the immune response of monkeys to SIV envelope proteins is thought to be different from the immune response of humans to HIV-1 [8]. Therefore, chimeric simian–human immunodeficiency viruses (SHIVs) which contain the HIV-1 envelope gene within a genetic background of SIVmac were originally developed by our group [9] and are now constructed in some laboratories and used for investigating the role of Env in viral infection, pathogenesis, and the host immune responses [10]. Some SHIV strains were reported to be acutely pathogenic and to induce rapid (within 3–4 weeks) and irreversible loss of circulating $CD4^+$ T cells, leading to AIDS-like disease in macaque monkeys [10–12]. A rapid and irreversible loss of peripheral $CD4^+$ T cells is the signature property of pathogenic SHIVs, which utilize the CXCR4 co-receptor and not SHIVs which utilize the CCR5 co-receptor. The target of the CXCR4-SHIV clone is the peripheral blood and such lymphoid organs as thymus, and the target of the CCR5-SHIV clone is the gut-associated lymphoid tissue [11,13,14]. Most HIV-1 strains transmitted between humans use CCR5 as their co-receptor. The lymphocyte subset targeted for elimination by primary HIV-1 infection is identical to that targeted by pathogenic CCR5-SHIV and not the lymphocyte subset targeted by CXCR4-SHIV [15,16]. However, CXCR4-using or, in some cases, dual-tropic (CCR5- and CXCR4-using) virus variants emerge later during disease. The emergence of HIV-1 variants that are able to use CXCR4 or several other co-receptors is correlated with a rapid decline in the number of peripheral $CD4^+$ T cells and progression to AIDS [17]. Therefore, it will be a useful approach to understanding human AIDS pathogenesis to examine an acute pathogenic SHIV strain utilizing CXCR4 or both CXCR4 and CCR5 in order to clarify the mechanisms by which circulating $CD4^+$ T lymphocytes are lost irreversibly in vivo. In this study, we used two SHIV molecular clones, which utilize both CXCR4 and CCR5 co-receptors, and examined their effects on thymopoiesis to compare the pathogenicities of acute and less pathogenic SHIVs having the same genetic origin.

2. Materials and methods

2.1. Animal experiments and viruses

Sixteen rhesus monkeys (*Macaca mulatta*) were used in this study. They were one 1-year-old juvenile (Mm1688), eight 3-year-old young monkeys (MM372, MM374, MM380, MM390, MM391, MM392, MM394 and MM396) and seven 5- to 8-year-old adults (MM244, MM300, MM307, MM308, MM310, MM313 and MM334). These monkeys were treated in accordance with the institutional regulations approved by the Committee for Experimental Use of Nonhuman Primate in the Institute for Virus Research, Kyoto University. All monkeys were confirmed to be free of simian immunodeficiency virus (SIV) and simian T-cell leukemia/lymphoma virus type 1 (STLV-1). We used two molecularly cloned viruses (SHIV-C2/1 [KS661] and SHIV-cl64) derived from the same original clone, SHIV-89.6, in this study. SHIV-C2/1 [KS661] is a molecular clone, which was constructed from the consensus sequence of SHIV-C2/1 (GenBank accession number AF217181). In cynomolgous monkeys, inoculation of SHIV-C2/1 causes a rapid and profound $CD4^+$ T cell decline within a couple of weeks, which is followed by miscellaneous opportunistic infections [12]. SHIV-cl64, which is a molecularly cloned virus derived from the SHIV-89.6P strain, is a less pathogenic virus. In SHIV-cl64-inoculated rhesus monkeys, the kinetics of plasma viral loads and $CD4^+$ T-cell counts were similar to those of the parental pathogenic virus SHIV-89.6P within the first 4 weeks post-inoculation. However, in these monkeys, the viral load gradually decreased, $CD4^+$ T-cell counts were restored almost to the their original state, and the virus failed to cause an AIDS-like disease [18]. In this study, eight macaques were intrarectally inoculated with 2000 $TCID_{50}$ (measured by CEMx174 cell line) of the acute pathogenic SHIV-C2/1 and four macaques were intrarectally inoculated with 200,000 $TCID_{50}$ of the less pathogenic SHIV-cl64. The two inocula sizes both correspond to about 10 MID_{50}. Four macaques were used as uninfected controls. Blood samples were periodically taken to monitor $CD4^+$ T-cell counts and to determine the plasma virus load. The acute pathogenic SHIV-C2/1-infected monkeys were euthanized at 3, 6, 13 and 27 dpi and the less pathogenic SHIV-cl64-infected monkeys were euthanized at 6, 13 and 27 dpi. Necropsy samples were taken to prepare thymus sections for histopathology, immunohistochemistry and DNA extraction, to obtain thymocytes for FACS analyses and to observe the differentiation of intrathymic progenitors in fetal thymus organ culture (FTOC).

2.2. Viral RNA loads in plasma

Virion-associated SHIV RNA loads in plasma were measured by real-time reverse transcription (RT)-PCR assay [18]. Total RNA was prepared from plasma (140 μl) of each monkey with a QIAamp Viral RNA kit (QIAGEN, Hilden, Germany). RT reactions and PCR were performed by a Platinum qRT-PCR ThermoScript One-Step System (Invitrogen, Carlsbad, CA) using the following primers for the *gag* region; SIV2-696F (5′-GGA AAT TAC CCA GTA CAA CAA ATA GG-3′) and SIV2-784R (5′-TCT ATC AAT TTT ACC CAG GCA TTT A-3′). A labeled probe, SIV2-731T (5′-Fam-TGT CCA CCT GCC ATT AAG CCC G-Tamra-3′; Perkin Elmer, Wellesley, MA), was used for detection of the PCR products.

These reactions were performed with a Prism 7700 Sequence Detector (Applied Biosystems, Foster City, CA) and analyzed using the manufacturer's software. For each run, a standard curve was generated from dilutions whose copy numbers were known, and the RNA in the plasma samples was quantified based on the standard curve. Under these conditions, the detection limit was 1000 copies/ml.

2.3. Peripheral $CD4^+$ T-cell counts

Whole blood samples were stained with two fluorescently labeled mouse monoclonal antibodies, fluorescein isothiocyanate (FITC)-conjugated anti-monkey CD3 (FN-18, BioSource Intl, Camarillo, CA) and phycoerythrin (PE)-conjugated anti-human CD4 (Nu-TH/I; NICHIREI, Tokyo, Japan). After haemolysis of the whole blood using lysing solution (Becton Dickinson, Franklin Lakes, NJ), each type of labeled lymphocytes was examined on a FACScan analyzer using Cellquest software (Becton-Dickinson). The absolute number of lymphocytes in the blood was determined by using an automated blood counter (F-820; Sysmex, Kobe, Japan).

2.4. Histopathological and immunohistochemical examinations

The thymuses obtained from sacrificed monkeys were fixed in 4% paraformaldehyde (PFA)–PBS (1 phosphate-buffered saline) overnight at 4 C, and embedded in paraffin wax for histopathological (hematoxylin–eosin staining) and immunohistochemistry studies. For immunohistochemistry, 4-μm sections were rehydrated and processed for 10 min in an autoclave in 1 mM EDTA (pH 8.0) to unmask the antigens, sequentially treated with TBS-Tween 20 and aqueous hydrogen peroxide, stained with anti-human CD4 mouse monoclonal antibody (NCL-CD4; Novacastra Laboratories, Ltd., London, United Kingdom, 1:40) or rabbit anti-terminal deoxynucleotidyl transferase (TdT) polyclonal antibody (DAKO Corp., Carpinteria, CA, 1:40) for 1 h, stained with an EnVision kit (DAKO) for 1 h and diaminobenzidine, rinsed in distilled water and counterstained with hematoxylin (DAKO).

2.5. Sample collection of thymocytes

Samples of thymus fragments obtained at serial necropsies were mechanically disrupted and separated with a 100 μm nylon mesh filter (Becton Dickinson). The obtained cells were used for surface staining, cell sorting and fetal thymus organ culture.

2.6. Quantitative analysis of provirus DNA in thymuses and peripheral blood mononuclear cells (PBMCs)

SHIV proviral DNA was quantitatively assayed with Platinum Quantitative PCR SuperMix-UDG (Invitrogen) for the SIV *gag* region using the same primers and probe as described in the section of viral RNA load in plasma. DNA samples were extracted directly from frozen thymus sections and PBMCs of each monkey with a QIAGEN DNeasy Tissue kit (QIAGEN) according to the manufacturer's protocol. For each run, a standard curve was generated from dilutions of a reference plasmid DNA sample containing the full genome of SHIV-cl64, which was quantified with a UV spectrophotometer.

2.7. Cell surface staining for flow cytometric analyses and cell sorting of obtained cells

Thymocytes were stained with FITC-anti-monkey CD3, PE-anti-human CD4, and allophycocyanin (APC)-anti-human CD8 (Leu-2a; Becton Dickinson). CD4 and CD8 thymocytes in the CD3 population (TN intrathymic progenitors) were sorted by FACSVantageSE (Becton Dickinson). Non-viable cells were excluded by forward and side scatters and propidium iodide (PI) staining. Sorted cells were reanalyzed to check their purity and were always found to be >99% pure. Thymocytes were also stained with FITC-labeled CD2 (39C1.5; Coulter), CD3, CD4 (Nu-TH/I; NICHIREI), CD8 (Leu-2a; Becton Dickinson), CD11b (Leu-11a; Becton Dickinson), CD20 (Leu-16; Becton Dickinson) and CD45RA (5H9; PharMingen) as lineage markers (Lin) and with PE-anti-human CD34 (563; Becton Dickinson).

2.8. Mice and fetal thymus organ culture (FTOC)

Pregnant C57BL/6 (B6) mice were purchased from Japan SLC (Shizuoka, Japan). Fetal thymus (FT) lobes obtained from fetuses 15 days postcoitum were cultured as described previously [19]. One murine thymic lobe and 2 10^3 cells of CD3 CD4 CD8 triple-negative (TN) thymocytes purified by the cell sorter were placed in RPMI 1640 medium in each well of a 96-well plate. Total volume of each well was 200 μl. The plates were centrifuged at 150 *g* for 5 min at room temperature and incubated in a plastic bag (Ohmi Oder Air Service, Hikone, Japan) containing 70% O_2, 25% N_2, and 5% CO_2 at 37 C. The medium was changed every 3 days. Cells from both inside and outside the FT lobe were harvested from three wells at each time point, and single cell suspensions were made for the analysis. Viable cells were counted by trypan blue dye exclusion, and then surface phenotypes were analyzed by FACSVantageSE. Non-viable cells were excluded by forward and side scatters and PI staining. In FTOC, TN thymocytes from uninfected monkeys matured into $CD4^+CD8^+$ double-positive (DP) cells. The differentiation started with DP cells (8.5%) on day 9 after co-culture and increased to over 70% by day 14 and remained at this level to day 19 (data not shown). Therefore, day 14 of co-culture was selected as the time for evaluating the development from TN thymocytes to DP cells [20].

3. Results

3.1. Kinetics of plasma virus loads and $CD4^+$ T cell numbers in peripheral blood

The kinetics of virus replication was similar in each monkey infected with the acute pathogenic SHIV-C2/1 (Fig. 1A-a) and in each monkey infected with the less pathogenic

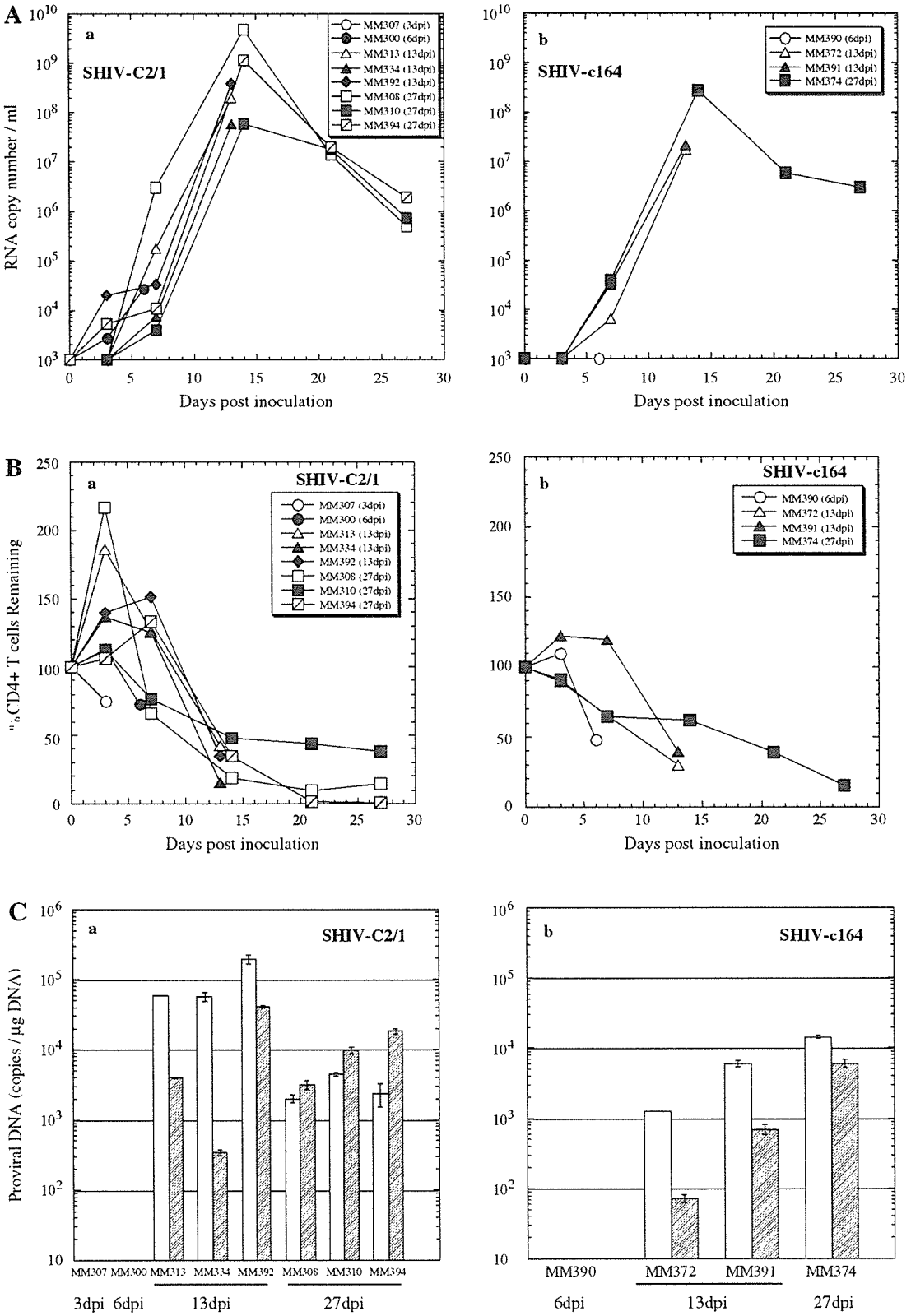

Fig. 1. (A) Time course of plasma virus RNA loads in SHIV-C2/1-infected (a) and SHIV-cl64-infected (b) monkeys. The detection limit of this assay was 1000 copies/ml. (B) Kinetics of peripheral $CD4^+$ T-cells counts of monkeys after inoculation with SHIV-C2/1 (a) and SHIV-cl64 (b). Values are expressed as a percent of the cell counts immediately before inoculation. (C) Amounts of proviral DNA in thymus tissues (striped bars) and PBMCs (white bars) from monkeys inoculated with SHIV-C2/1 (a) and SHIV-cl64 (b). Viral loads were measured by quantitative DNA PCR in duplicates.

SHIV-cl64 (Fig. 1A-b), although the mean peak level of plasma RNA in the SHIV-cl64-infected monkeys was less than that in the SHIV-C2/1-infected monkeys. Viral RNAs started to appear in the plasma within a week. The plasma viral loads reached their peak levels, more than 10^7 viral RNA copies per ml, at the second week, and fell to about 10^6 viral RNA copies per ml at 27 dpi. In most of the infected monkeys, the numbers of peripheral blood $CD4^+$ T cells declined by more than 50% in about 2 weeks (Fig. 1B–a and b). The $CD4^+$ T cells declined in these monkeys, as the viruses actively replicated. The kinetics of viral loads and the relative number of the $CD4^+$ T cell numbers of the monkeys are in good agreement with those previously reported for longer-term SHIV-C2/1 infections of cynomolgous monkeys [12] and for longer-term SHIV-cl64 infection of rhesus monkeys [18].

3.2. Amounts of provirus DNA in PBMCs and thymus sections

In the monkeys infected with the SHIV-C2/1 (Fig. 1C-a), provirus DNA was undetectable in PBMCs and thymus sections at 3 and 6 dpi, but was detected in these tissues at high levels at 13 and 27 dpi. The amount of virus in the thymus sections was lower than that in PBMCs at 13 dpi, and higher than that in PBMCs at 27 dpi. In the monkeys infected with the SHIV-cl64, the virus was also detected in PBMCs and the thymus section from 13 dpi, although at lower levels than in the monkeys infected with the SHIV-C2/1. The amount of virus in thymus sections was lower than that in PBMCs at 13 and 27 dpi (Fig. 1C-b).

3.3. $CD4^+$ and TdT^+ cell depletion in thymus of acute pathogenic SHIV-infected monkeys

Thymic morphology in the SHIV-C2/1-infected monkeys was unaffected at 3 dpi and at 6 dpi (data not shown) and hardly affected with discernible corticomedullary junction at 13 dpi as shown by hematoxylin–eosin (H&E) staining (Fig. 2A-a, upper panel, white arrow). Severe involution, decreased cell density, especially in the cortex region (Fig. 2A-a, lower panel, black arrow), and no discernible corticomedullary junction were observed at 27 dpi in the SHIV-C2/1-infected monkeys. Immunohistochemical analyses revealed a nearly unaffected distribution of $CD4^+$ cells in the thymic medulla (black arrow) and cortex (white arrow) at 13 dpi (Fig. 2A-b, upper panel) but a profound depletion of $CD4^+$ cells in the thymic medulla (black arrow) to the cortex (white arrow) at 27 dpi (Fig. 2A-b, lower panel). TdT^+ cells were not decreased up to 13 dpi (Fig. 2A-c, upper panel, black arrow), but they were strongly decreased at 27 dpi (Fig. 2A-c, lower panel). TdT^+ cells are immature T cells that are involved in the regulation of T-cell receptor (TCR) gene rearrangement and are mainly distributed in the thymic cortex. In contrast, no clear alteration in thymic morphology was observed in the SHIV-cl64-infected monkeys (Fig. 2B-a–c).

3.4. Depletion of immature thymocytes in acute pathogenic SHIV-infected monkeys

The fraction of DP thymocytes in SHIV-C2/1-infected monkey thymuses was more than 70% at 3 and 6 dpi, an average of 69% (range 40.5–83.4%) at 13 dpi and an average of 10.5% (range 1.5–26.4%) at 27 dpi (Fig. 3b). The fraction of DP thymocytes in SHIV-cl64-infected monkey thymuses, like that in thymuses of uninfected monkeys, remained at about 80% (Fig. 3a and c). Further, the fraction of $CD34^+$ thymocytes that were earliest progenitors significantly decreased from about 20% (the level in uninfected monkeys) to less than 8% at 13 and 27 dpi in SHIV-C2/1-infected monkeys although those in SHIV-cl64-infected monkeys decreased insignificantly (Fig. 4).

3.5. Impaired differentiation of intrathymic progenitors from acute pathogenic SHIV-infected monkeys

TN thymocytes were sorted electrically by FACSVantageSE and cultured in FTOC system to determine whether the thymopoietic potential of intrathymic progenitors derived from the infected monkeys was affected by SHIV infection in vivo (Fig. 5). In MM307, one of the SHIV-C2/1-infected monkeys, neither plasma virus nor proviral DNA was detected in the thymus section at 3 dpi. In this monkey, 64.7% of the cells in FTOC differentiated to DP cells. This efficiency is comparable to that observed in the thymus of the uninfected monkeys. MM300, another SHIV-C2/1-infected monkey, was sacrificed at 6 dpi. The ability of TN thymocytes from this monkey to differentiate in FTOC was slightly diminished. The fraction of cells that developed to DP cells was 23.0%. The fractions of cells that differentiated to DP cells were quite lower in the SHIV-C2/1-infected monkeys sacrificed at 13 and 27 dpi. In the monkeys sacrificed at 13 dpi (MM313, MM334 and MM392), the fractions of cells that differentiated to DP cells were 5.4%, 25.5% and 2.1%, respectively. In the monkeys sacrificed at 27 dpi (MM394, MM308 and MM310), the fractions of cells that differentiated to DP cells were 7.9%, 0.0% and 5.2%, respectively (Fig. 5A-a). In thymus from the SHIV-cl64-infected monkey sacrificed at 6 dpi (MM390), the fraction of cells that differentiated to DP cells did not increase as much as it did in the uninfected monkeys (44.4%). However, in thymuses from the SHIV-cl64-infected monkeys sacrificed at 13 dpi (MM372 and MM391) and at 27 dpi (MM374), the fractions of cells that differentiated to DP cells were equal to or higher than those differentiated in uninfected monkeys (73.8% in MM372, 75.1% in MM391, and 70.1% in MM374) (Fig. 5A-b). Fig. 5B shows the proliferation of an initial inoculation of 2 10^3 TN thymocytes from SHIV-C2/1-infected monkeys (a) and SHIV-cl64-infected monkeys (b) in FTOC. TN thymocytes taken from the uninfected monkeys (MM244 and MM396; shown in both panels of Fig. 5B) increased about 15-fold (3 10^4 cells) at 2 or 3 weeks in the culture. TN thymocytes taken from two of the SHIV-C2/1-infected monkeys (MM307 and MM300) at 3 and 6 dpi increased about eight-fold at 3 weeks. TN thymocytes taken

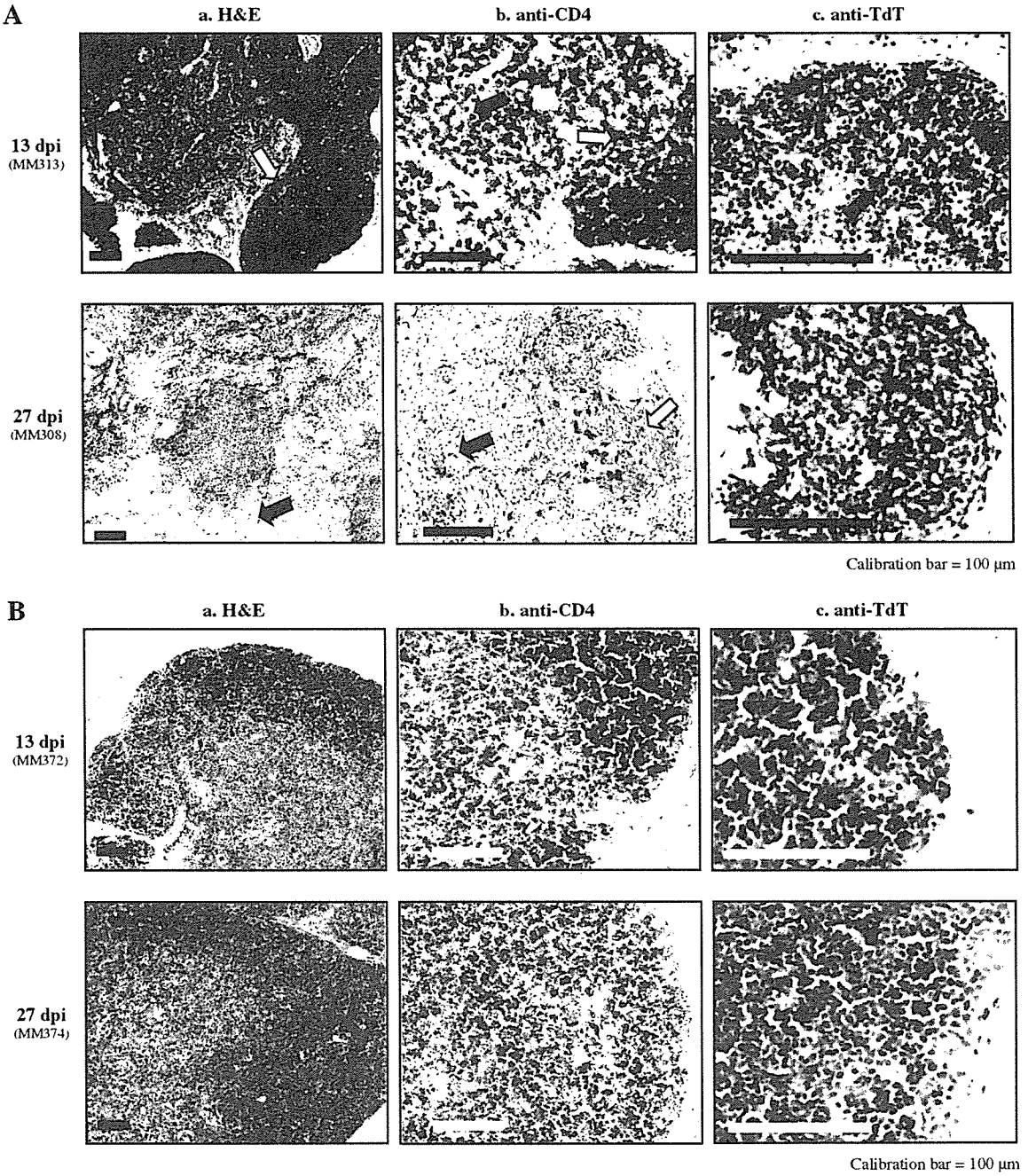

Fig. 2. Histopathological changes of the infected thymuses during the SHIV-C2/1 (A) and the SHIV-cl64 (B) infection. Fixed tissue samples were stained with hematoxylin–eosin (H&E) (a) and immunostained with an anti-human CD4 monoclonal antibody (b) and with an anti-TdT polyclonal antibody (c), at the indicated times. The upper panels are thymuses of 13 dpi and the lower panels are thymuses of 27 dpi.

from the SHIV-C2/1-infected monkeys at 13 and 27 dpi hardly proliferated at all (Fig. 5B-a). Most of the TN thymocytes taken from the SHIV-cl64-infected monkeys increased more than did the TN thymocytes taken from the uninfected monkeys except for the MM390 sacrificed at 6 dpi (Fig. 5B-b). The absolute numbers of cells that differentiated to DP cells at 14 days in FTOC were calculated from the above data (Fig. 5C). Both the ability to differentiate and the proliferation of TN thymocytes from the SHIV-C2/1-infected monkeys were seriously impaired resulting in an almost complete defect of DP cells production at 13 and 27 dpi. On the contrary, differentiation and proliferation of TN thymocytes from SHIV-cl64-infected monkeys were not affected or were accelerated although they were slightly reduced at 6 dpi, as they were in the SHIV-C2/1-infected monkeys.

4. Discussion

A comparison of the effects of different pathogenic SHIVs can help to understand the AIDS pathogenesis in vivo [21,22].

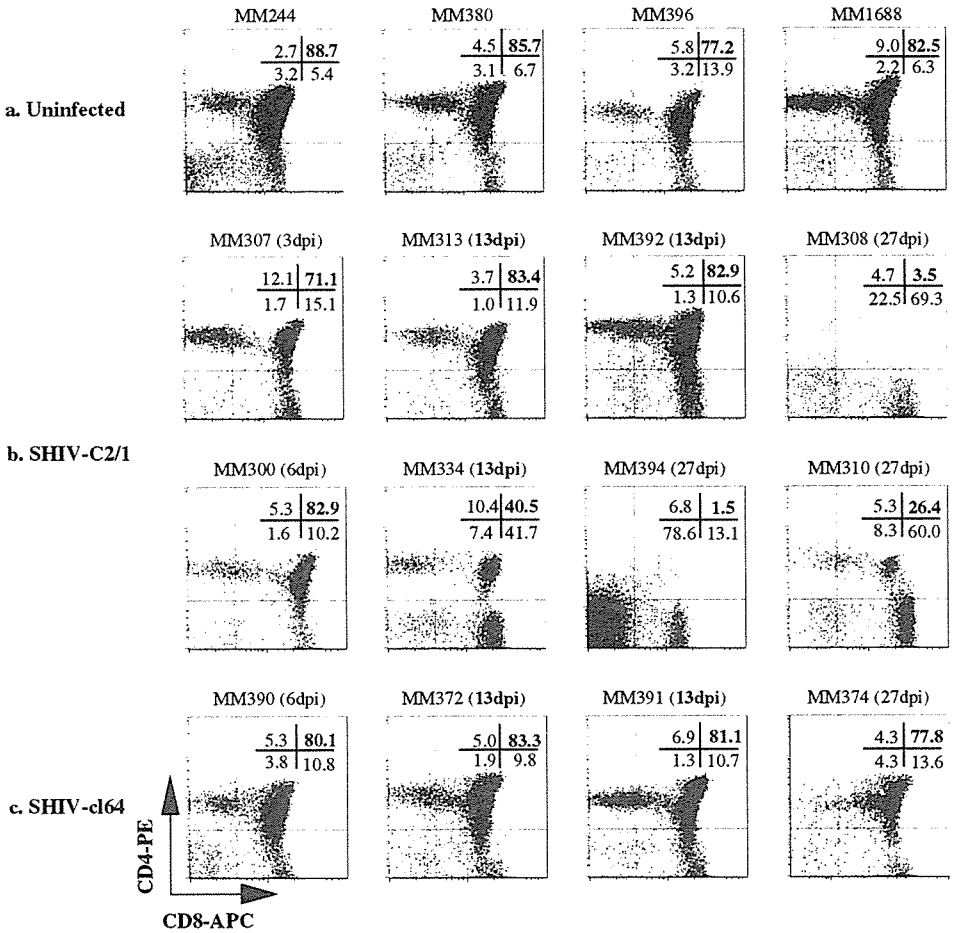

Fig. 3. Thymocytes were stained with surface markers for CD4 and CD8 and analyzed by FACSVantageSE. (a) Uninfected monkeys. (b) SHIV-C2/1-infected monkeys. (c) SHIV-cl64-infected monkeys. The decrease in the subpopulation was significant at 13 and 27 dpi in the SHIV-C2/1-infected monkeys but not in the SHIV-cl64-infected monkeys.

The acute pathogenic SHIV-C2/1 infection is clinically characterized by a constant high viral load and a rapid and irreversible peripheral circulating $CD4^+$ T-cell depletion within a couple of weeks [12], while the less pathogenic SHIV-cl64 is clinically characterized by a gradual decrease of the viral load and the recovery of $CD4^+$ T-cell counts after an initial decline [18]. In this study, the differences observed in peripheral blood were less significant than the big differences observed in thymuses. Direct killing of infected mature $CD4^+$ cells seems to explain the initial decrease of circulating $CD4^+$ cells in the first 4 weeks in both the SHIV-C2/1- and SHIV-cl64-infected monkeys. However, histopathological analyses of the infected thymuses imply that the virulence against the immature cell populations is quite different between SHIV-C2/1 and SHIV-cl64.

Our finding that TN thymocytes from the SHIV-C2/1-infected monkeys at 13 and 27 dpi did not increase in number nor differentiate to DP cells in FTOC indicates that thymopoiesis was strongly disturbed at the level of thymocyte progenitor function. It is unlikely that the impairment was caused by active replication of the virus carried by the thymocytes during the culture. Viral copy number in the culture supernatant remained in the range 10^3–10^5 copies/ml during the FTOC, while it is generally more than 10^9 copies/ml in virus replicating PBMC culture. Furthermore, TN thymocytes from uninfected monkeys that were inoculated with an excessive amount of infectious virus (1 moi) showed hardly any reduction of thymopoiesis in FTOC (data not shown). In contrast, thymopoiesis was completely impaired in the SHIV-C2/1-infected monkeys. Therefore, the impaired thymopoiesis in FTOC observed in this study is considered to be caused by the change of the TN cell populations in infected monkeys.

What mechanisms might cause the impairment of the differentiation and proliferation of T-cell progenitors in acute pathogenic SHIV-infected monkeys? First, we suspect that it is because the infectivities of the two viruses are quite different. In fact, the viral infectivity to an established cell line M8166 of the SHIV-C2/1 is several logs higher than that of the SHIV-cl64 in vitro (data not shown). Furthermore, the inoculated $TCID_{50}$ dose of SHIV-cl64 needed to be 100-fold higher than that of SHIV-C2/1 to obtain comparable MID_{50} with intrarectal infection. The higher basic infectivity of SHIV-C2/1 is probably the main reason it impaired thymopoiesis more than SHIV-cl64.

Second, the loss of the ability of TN thymocyte to differentiate in infected monkeys can be partly explained by the

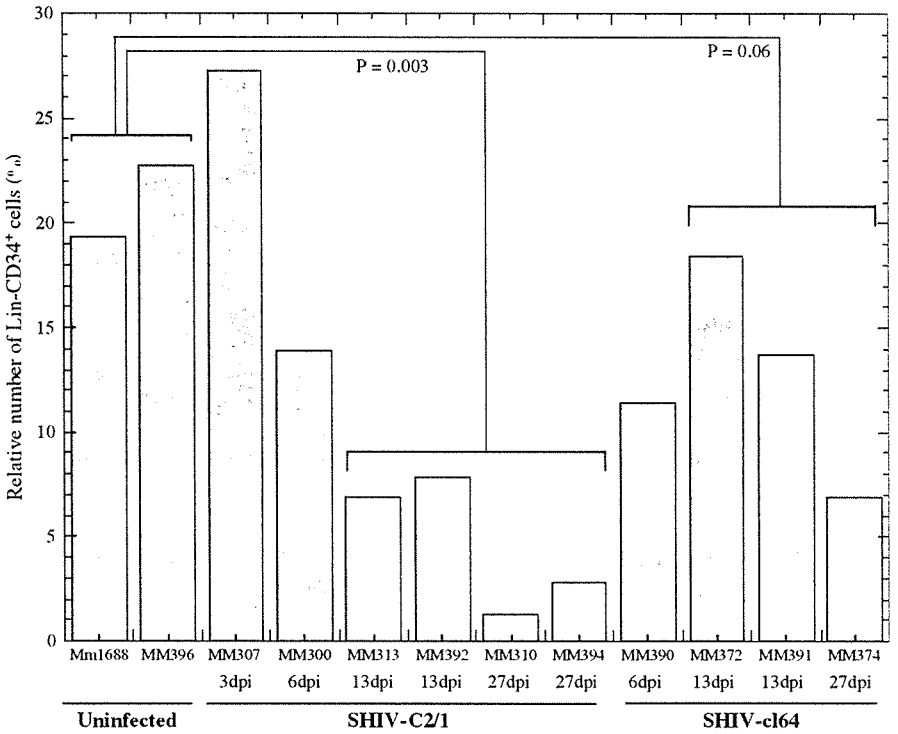

Fig. 4. Changes of relative cell percent in the $CD34^+$ subpopulation in the lineage marker-negative thymocytes at the indicated times in uninfected monkeys. SHIV-C2/1-infected monkeys and SHIV-cl64-infected monkeys.

observation that $CD34^+$ hematopoietic precursors significantly decreased in the thymus at 13 and 27 dpi in the SHIV-C2/1-infected monkeys. The earliest progenitors in the thymus are $CD34^+$ cells in TN thymocytes excluding the cells having CD11b, CD20 and other T-cell lineage markers. CD34 is a marker of pluripotent hematopoietic stem cells. $CD34^+$ cells in the thymus are the cells that have immigrated to the thymus from bone marrow and that have the potential to differentiate from TN thymocytes to mature cells [23]. These results, together with the finding that SHIV impairs hematopoiesis in early bone marrow in monkeys [24], suggest that thymopoiesis is affected before or just after immigration to the thymus in SHIV-C2/1-infected monkeys. Also, the relative number of each subpopulation in TN thymocytes may be changed by the acute pathogenic SHIV infection. TN thymocytes contain several subpopulations which are not only T-cell progenitors but also thymic dendritic cells, thymic stromal cells, etc. [25]. Further analyses are needed to clarify the relation between the change of subpopulations and the impaired thymopoiesis.

The increase in the number of TN thymocytes from the SHIV-cl64-infected monkeys at 13 and 27 dpi, and the rate at which they differentiated to DP cells were equal to or more than the values observed for TN thymocytes from the uninfected monkeys. However, at 6 dpi, the increase and rate of differentiation were lower for TN thymocytes from the SHIV-cl64-infected monkeys than they were for the TN thymocytes from uninfected monkeys. This suggests that thymopoiesis in the less pathogenic SHIV-infected monkeys was also impaired just after the infection but it was restored and enhanced subsequently. It is interesting that impairment of thymopoiesis started at 6 dpi although the proviral DNA was hardly detected in the thymuses in both types of virus-infected monkeys. Because plasma viral RNA starts to be detected at 6 dpi, virus carried by the circulation might be responsible for the impaired thymopoiesis at the very early stage of infection.

Generally, co-receptor usage of the virus is important for AIDS pathogenesis because it is associated with cell tropism. CXCR4-utilizing viruses preferably infect and decrease naive CD4 T cells, whereas CCR5-utilizing viruses preferably infect and decrease memory CD4 T cells [26]. It was reported that CXCR4-utilizing SHIVs are more pathogenic in the thymus [13], whereas CCR5-utilizing SHIV/SIV/HIVs preferably decrease intestinal CD4 T cells [11,15,16,27]. The SHIV-C2/1, which uses both CXCR4 and CCR5, is not only strongly pathogenic to the thymus, as was shown in this study, but it was also shown to decrease the intestinal CD4 T cells from the early stage of infection [28]. Recently, it was reported that the role of thymus is limited in the pathogenesis of SIVmac, a CCR5-utilizing virus [29]. All these observations can be simply explained by the relation among viral co-receptor usage, cell tropism and target organ. CXCR4-utilizing virus targets the thymus including more naive CD4 T cells and CCR5-utilizing virus targets intestinal tract including more memory CD4 T cells.

A previous report indicated that the thymus contributes little to peripheral blood T-lymphocyte population [30], that is, a drastic CD4 depletion in peripheral blood cannot be explained by impaired thymopoiesis. In this study, the decrease of peripheral blood CD4 cells within the first 4 weeks was